UNIVERSITY OF CAMBRIDGE
Department of Engineering

Performance Evaluation of CDL Channel Models in a 5G NR Downlink End-to-End Simulation

Author Name: Ian Cho

Supervisors: Prof. Albert Guillen I Fabregas, Alexander Hamilton (Nokia)

Date: May 2025

I hereby declare that, except where specifically indicated, the work submitted herein is my own original work.

Signed Ian Cho *date* 02/06/25

Acknowledgements

I would like to express my sincere gratitude to my supervisors, Prof. Albert Guillen i Fabregas and Alexander Hamilton at Nokia Bell Labs, for their continuous guidance and support throughout the course of this project. I am especially grateful for their willingness to meet weekly, and their insights and invaluable feedback have been significant in shaping both the direction and depth of my research.

I would also like to thank Tugce Kobal at Nokia Bell Labs, who has also generously dedicated her time every week to provide us with helpful discussions and technical advice. A special thank you to Kelvin, Krish, and Tian, who are also working closely with this project, for providing helpful insights, logistical reminders, and much more.

I am grateful to friends from high school, university, and church for their camaraderie and motivation, especially during the more challenging periods of this journey. I also extend my thanks to the teaching and administrative staff at the Engineering Department and Pembroke College for all the academic, pastoral, and financial support I received throughout my studies.

Lastly, I wish to thank my family for their constant encouragement, patience, and belief in me, without any of which it would not have been possible.

Technical Abstract

Performance Evaluation of Clustered Delay Line Channel Models in a 5G NR Downlink End-to-End Simulation

Ian Cho - University of Cambridge - Pembroke College
Supervised by: Prof. Albert Guillen i Fabregas, Alexander Hamilton (Nokia)

Overview

This dissertation presents a simulation-based evaluation of 5G New Radio (NR) downlink performance under standardised Clustered Delay Line (CDL) channel models, as defined in 3GPP TR 38.901. The work investigates the implications of using CDL-based fading environments on link-layer throughput performance, focusing on multi-layer Multiple Input Multiple Output (MIMO) transmission with varying User Equipment (UE) mobility (i.e. Doppler shifts) under realistic assumptions.

Modern wireless systems must adapt transmission strategies to dynamic propagation environments. Features at the physical layer, such as Hybrid Automatic Repeat Request (HARQ) and Channel State Information (CSI) feedback, offer adaptive schemes to improve the number of successful transport block transmissions, e.g. Block Error Rate (BLER), whilst CDL models offer spatially-resolved fading structures that reflect real-world propagation in urban macro and micro scenarios. This project develops a MATLAB-based end-to-end 5G NR simulation framework, motivated by previous related studies, leveraging the 5G Toolbox to integrate real-world features such as HARQ, Channel Quality Indicator (CQI)/Precoding Matrix Indicator (PMI)/Rank Indicator (RI) feedback and channel estimation.

Methodology

Using 3GPP-defined standardised parameters stated in industry reports for development towards a TR 38.753 CDL model for the yet-to-be-published Release 19, a link-level simulation framework is implemented to support varying transmitter and receiver antenna configurations (up to 8-layer MIMO). Each downlink transmission feature, such as HARQ, CSI feedback, and channel estimation, is systematically implemented, and its performance is evaluated and compared with existing literature to validate the simulation framework.

Then, using a realistic assumption, CDL-A through CDL-E profiles are tested along with varying Doppler shifts and MIMO configurations. Although features like CQI and RI for adaptive Modulation Coding Schemes (MCS) and adaptive layering are implemented and their performance is investigated, they were fixed for clearer benchmarking. This framework also supports HARQ retransmissions, type-1 codebook-based PMI selection, perfect or least squares-based channel estimation, and subarray virtualisation to emulate a large number of antenna elements to a limited number of CSI ports. Simulations sweep

SNR values from -5 dB across 1000 slot realisations per point, using Monte Carlo averaging to ensure statistical reliability.

Key Findings

The simulation results highlight several key performance trends observed under standardised CDL channel models. First, throughput degrades in spatially rich CDL scenarios (e.g. urban macro scenarios compared to sparser rural cases). Notably, CDL profiles with narrower angular spreads yield higher throughput when the base station beam is closely aligned with the UE. The effect of UE mobility was also investigated, with throughput degrading at higher speeds due to inaccurate channel estimations, particularly when temporal variations are not considered.

MIMO layer scaling further revealed that whilst increasing the number of layers can improve the capacity, the gains are strongly dependent on accurate CSI and channel modelling, where inaccuracy suffers from the saturation of maximum channel rank. The implementation of subarray virtualisation showed that larger transmitter antenna arrays, with the same number of layers, ideal CSI feedback, and ideal channel estimation, result in a throughput loss of approximately 7-11 dB compared to smaller arrays.

Lastly, comparisons with vendor-reported benchmarking results indicate that, whilst simulation trends align between MIMO layers, results diverge due to simplified channel estimation and saturation of channel rank without the implementation of TR 38.753 CDL-defined features such as ray splitting.

Conclusion

The study, whilst aligned with 3GPP standards, has certain limitations that affect the direct applicability of its results to real-world systems. First, idealised assumptions about the hardware, RF non-linearities and protocol stack latencies were not considered, resulting in optimistic performance compared to practical deployments. Second, quantisation, predictive lag, and delay for CSI feedback were simplified, and RI and CQI were fixed for controlled benchmarking. This impacts the precoding accuracy and system capacity. Lastly, a least squares channel estimator was used, which is invariant to channel noise and temporal effects, such as Doppler. Hence, performance, particularly at high SNRs, was overestimated. Despite these limitations, when compared with industry-reported data, there was alignment in demonstrating trends between different MIMO configurations and transmission feature effects such as HARQ. Therefore, these findings still remain highly relevant to real-world system design and contribute meaningfully to ongoing discussions on CDL benchmarking for Release 19 and beyond.

Contents

List of Figures

List of Tables

List of Abbreviations

3GPP	Third Generation Partnership Project
5G	Fifth Generation
6G	Sixth Generation
AAV	Antenna Array Vector
ACK	Acknowledgement
AoA/AoD	Angle of Arrival/Angle of Departure
AWGN	Additive White Gaussian Noise
AWS	Amazon Web Services
BLER	Block Error Rate
CDL	Clustered Delay Line
CP	Cyclic Prefix
CS	Configured Scheduling
CSI	Channel State Information
CSI-RS	Channel State Information Reference Signal
CQI	Channel Quality Indicator
DCCH	Downlink Control Channel
DCI	Downlink Control Information
DL-SCH	Downlink Shared Channel
DM-RS	Demodulation Reference Signal
DTCH	Downlink Traffic Channel
eMBB	enhanced Mobile Broadband
FR	Frequency Range
gNB	Next Generation Node B (base station)
HARQ	Hybrid Automatic Repeat Request

LOS/NLOS	Line-of-Sight/Non-Line-of-Sight
LTE	Long Term Evolution
MCS	Modulation and Coding Scheme
MIMO	Multiple Input Multiple Output
MMSE	Minimum Mean Square Error
mMTC	massive Machine Type Communication
mmWave	millimetre Wave
NACK	Negative Acknowledgement
NR	New Radio
NZP	Non-Zero Power
OFDMA	Orthogonal Frequency-Division Multiplexing
PBCH	Physical Broadcast Channel
PDCCH	Physical Downlink Control Channel
PDSCH	Physical Downlink Shared Channel
PMI	Precoding Matrix Indicator
QoS	Quality of Service
RI	Rank Indicator
RV	Redundancy Version
SCS	Subcarrier Spacing
SNR	Signal-to-Noise Ratio
SU/MU	Single-User/Multi-User
TDL	Tapped Delay Line
UE	User Equipment
URLLC	Ultra-Reliable Low-Latency Communication
ZF	Zero-Forcing

1. Introduction

1.1 Motivation

Wireless communication has evolved rapidly over the past decade. The transition from LTE to 5G New Radio (NR) has introduced a major leap in how data is transmitted and handled, especially at the physical layer. Whilst LTE laid the groundwork with techniques like Orthogonal Frequency-Division Multiplexing Access (OFDMA) and Multiple Input Multiple Output (MIMO) [1, Chapter 4], 5G NR has been designed further, introducing key concepts like millimetre-wave communication, network slicing, and massive MIMO, to address a wide range of new use cases [1, Chapters 1, 5, 11]. This includes enhanced Mobile Broadband (eMBB), Ultra-Reliable Low-Latency Communication (URLLC), and massive Machine-Type Communication (mMTC), all aimed at meeting the increasingly diverse demands of next-generation networks [1, Chapter 1, pp. 2–4].

In 5G NR, the downlink transmission refers to the flow of data from the base station (gNB) to the user equipment (UE) and conversely for uplink transmission. However, the downlink often carries the majority of user traffic, such as video streaming and web browsing. It is built around the Physical Downlink Shared Channel (PDSCH), which is facilitated by centralised downlink scheduling procedures at the gNB, as defined in 3GPP TS 38.214 [2].

The 3rd Generation Partnership Project (3GPP) is the organisation responsible for standardisation, which aims to create an international way forward, including the 5G NR physical layer. Through centralised scheduling, the gNB gains full visibility into user demands, channel conditions, and resource availability, allowing for the dynamic allocation of time-frequency resources, adaptive modulation, and the application of advanced features such as Hybrid Automatic Repeat Request (HARQ) retransmissions and MIMO precoding. As a result, PDSCH offers a rich area for performance optimisation, particularly under realistic channel conditions with varying user load.

In contrast, the uplink generally involves lower data rates and simpler transmission schemes due to constraints at the UE. Given the higher traffic demand, complexity, and industry focus, this project concentrates on evaluating downlink performance through metrics of throughput and Block Error Rate (BLER). However, the performance of this channel depends heavily on the characteristics of the spatial environment - this is why accurate channel modelling is necessary.

To support consistent and realistic performance evaluations, 3GPP introduced a set of standardised channel models in TR 38.901 [3]. These include both Tapped Delay Line (TDL) and Clustered Delay Line (CDL) models. TDL models represent channel behaviour using independent fading taps with delay and power profiles, making them suitable for scenarios where angular domain effects are less critical. On the other hand, CDL models account for defined angle spreads and spatial consistency across antenna elements by representing multipath environments using clusters of paths, where each cluster corresponds to a group of components arriving at the same location at similar times. This makes them particularly valuable for modelling multi-antenna systems and beamforming within

MIMO systems. Studies such as [4] have demonstrated the relevance of CDL models for evaluating beamforming and Multi-User (MU)-MIMO performance.

Whilst CDL models are commonly used in industry-standard evaluations due to their ability to reflect real-world multipath, angular spread, and mobility effects in urban and suburban deployments, academic studies often favour simpler models, such as TDL or Rayleigh fading, due to their lower complexity. For example, [5] highlights the use of TDL-A/B/C downlink 5G MIMO performance evaluation but focuses on CDL model behaviour. In contrast, recent 3GPP RAN4 development investigates the demodulation performance on CDL models [6, Section 7.16.2]. As a result, there still remains limited research that has explored the physical-layer impact of specific CDL profiles in detail, especially in realistic scenarios.

This project aims to bridge the gap between industry and academia. By building a MATLAB-based simulation of an end-to-end 5G NR downlink system and incorporating features such as OFDM modulation, HARQ, and MIMO precoding as specified by 3GPP, it provides a controlled and industry-standard aligned environment to evaluate the impact of different CDL scenarios under specific channel conditions. The next section now outlines the specific objectives and approach taken.

1.2 Project Objectives and Approach

The primary objective of this project is to evaluate the performance of 5G NR downlink systems under a range of standardised Clustered Delay Line (CDL) channel models, using end-to-end simulations developed with MATLAB 5G Toolbox [7]. The project specifically focuses on analysing the behaviour of the Physical Downlink Shared Channel (PDSCH) under a Signal-to-Noise Ratio (SNR) sweep, subject to varying channel conditions, MIMO configurations, and user mobility scenarios.

To achieve this, this dissertation aims to:

- Construct a controlled but flexible simulation framework to model an end-to-end PDSCH 5G NR system, evaluating different performance metrics, such as PDSCH throughput and Block Error Rate (BLER) and compare with existing studies and industry reports to ensure validity.
- Investigate and analyse performance of different CDL profiles (CDL-A, CDL-B, CDL-C). Each of these profiles models different real-world scenarios for spatial characteristics and delay spreads.
- Explore how changes in MIMO configurations (i.e. antenna configuration like MIMO layers) and user mobility speeds affect system performance.
- Assess the extent to which CDL-defined channel environments influence the practical gains of spatial multiplexing in typical deployment scenarios and explain certain trends or trade-offs that may occur.

This project takes a MATLAB simulation-based approach, implementing an end-to-end 5G NR downlink system. Key physical layer components such as OFDM modulation, channel coding, HARQ processing, and MIMO precoding are integrated in accordance with 3GPP standardised specifications [2], [3], [8], [9]. Performance metrics, such as

throughput and block error rate (BLER), are computed and graphically represented across a range of SNR values, assessing performance under varying channel conditions.

Then, the simulation results are analysed to discuss certain trends in the data and parameter sensitivities with their respective trade-offs. These results are compared, where relevant, against 3GPP documentation in TS 38.104 [10], TR 38.901 [3] and industry-reported benchmarks in Table B.1 to provide real-world context and validation of these results. Through this, the analysis supports the objective of a better understanding of CDL channel model behaviour, its implications for performance, and reliability for the current and future wireless systems.

1.3 Report Structure Overview

This dissertation is structured as follows:

- **Chapter 1 - Introduction:** introduces the background of 5G NR, motivation, aims and scope of work for the project, as well as providing a brief overview of the report structure.
- **Chapter 2 - Background and Literature Review:** presents a detailed overview of the 5G NR physical layer, how MIMO techniques are used in 5G, and different channel models with a focus on CDL profiles. It also reviews existing simulation-based studies and relevant industry reports from 3GPP to provide real-world context and highlight the motivation.
- **Chapter 3 - Methodology:** describes the simulation setup, which includes the system configuration, channel model, parameter ranges, and performance metrics measured across different scenarios.
- **Chapter 4 - Results and Discussion:** presents the simulated results, including throughput and BLER, then interprets the results, identifying key trends, behaviours, and trade-offs in data. Makes critical comparisons with existing work and industry data to provide context and validity of data.
- **Chapter 5 - Conclusion:** summarises the initial project aims and scope along with the key findings and contributions of the project. It outlines the limitations of the project simulation and also potential areas of development for future work.

2. Background and Literature Review

2.1 5G Physical Layer Overview

The 5G physical layer is designed to support a wide range of different deployment scenarios, such as eMBB, URLLC, and mMTC as mentioned in Section 1.1. This is accomplished through various techniques, like scalable numerologies and bandwidth [8, Sec. 4.2], adaptive modulation [2, Sec. 5.1], and advanced multi-antenna techniques using MIMO [2, Sec. 6]. 5G NR operates in two main frequency ranges: Frequency Range 1 (FR1), covering sub-6 GHz bands, and Frequency Range 2 (FR2), covering millimetre wave (mmWave) frequencies from 24.25 GHz upwards [10, Sec. 5.2].

LTE, the predecessor, introduced key concepts that 5G NR builds upon, for example, the use of OFDMs with cyclic prefixing that supports both frequency and time division duplexing [11, Sec. 6.2.3]. 5G NR, however, allows for scalable subcarrier spacing of ranges $15\text{kHz} * 2^n$, where $n \in \{0, 1, 2, 3, 4\}$, unlike LTE, which uses a fixed subcarrier spacing of 15 kHz. This enables adaptation to different latency and bandwidth needs, supporting up to 100 MHz in FR1 (sub-6 GHz) and up to 400 MHz in FR2 (mmWave). A key focus of this project lies within the evaluation of downlink performance, particularly through the Physical Downlink Shared Channel (PDSCH). It is useful to examine the structure and mapping of downlink channels within the physical layer and understand how physical resources are utilised in practice.

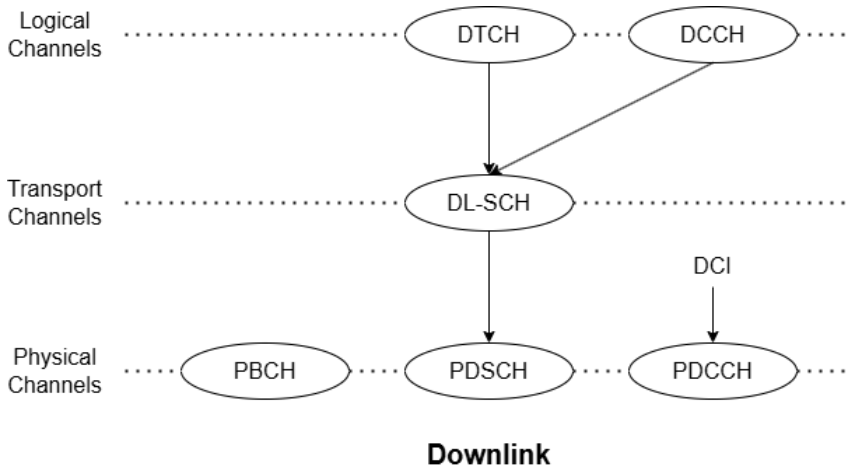

Figure 2.1: Simplified mapping between logical, transport, and physical channels in 5G NR downlink transmission, adapted from [1, Chapter 6, Figure 6.11].

As shown in Figure 2.1, the downlink data transmission path [8, Sec. 6] begins at the logical layer, which includes the Dedicated Traffic Channel (DTCH) for user data and the Dedicated Control Channel (DCCH) for signalling specific to a given user equipment (UE). Then, these logical channels are mapped to the Downlink Shared Channel (DL-SCH) at the transport layer, which serves as the primary transport mechanism for user data and control messages. The DL-SCH supports features such as HARQ, dynamic scheduling, and link adaptation [12, Sec. 6.1.3.2], which will be discussed further in Section 2.2.

At the physical layer, the DL-SCH is transmitted via the PDSCH, which handles a majority of the data transmitted in 5G NR. Alongside, the Physical Downlink Control Channel (PDCCH) controls the dynamic scheduling of the data allocated by the gNB. This delivers Downlink Control Information (DCI) which informs the UE of resource allocation, Modulation and Coding Scheme (MCS), and HARQ status, in which return allows it to measure the Channel Quality Indicator (CQI), to send back to the gNB. In addition, the Physical Broadcast Channel (PBCH), which is shown for completeness, exists for the initial access to the broadcast system information, but is not involved in any data transfer or user-specific scheduling and hence lies outside the scope of this project.

This layered structure between logical, transport and physical channels, along with the dynamic scheduling process of 5G NR downlink, allows the gNB to respond to rapidly changing channel conditions and user demands, which represents real-life scenarios accurately. This makes the PDSCH a critical point of performance optimisation, especially when analysed under standardised fading conditions as described by the CDL models [3, Sec. 7.7.1] discussed in Section 2.4.

2.2 Downlink Transmission Features

Downlink transmission via the PDSCH from the DL-SCH is supported by several adaptive features to improve link-level robustness and maximise spectral efficiency [12, Sec. 6.1.3.2]. These features include Hybrid Automatic Repeat Request (HARQ), dynamic scheduling, and link adaptation, which operate in conjunction to ensure that data transmitted is delivered effectively, even under dynamic channel conditions.

2.2.1 HARQ

HARQ is a retransmission mechanism that combines forward error correction (FEC) with selective retransmissions. Upon receiving a transport block via the PDSCH, the UE performs decoding and returns an acknowledgement (ACK) or negative acknowledgement (NACK) back to the gNB, indicating whether it can correctly decode the transmission. If a NACK is received, the gNB retransmits the block using a different redundancy version (RV), for which the standard RV sequence is $\{0, 2, 3, 1\}$, as defined in TS 38.214 [2], which determines the subset of coded bits. This allows the UE to perform soft combining of previously received RVs to improve the likelihood of successful decoding.

As shown in Figure 2.2, transmission of data block one results in an ACK leading to transmission of data block two, which results in a NACK. The gNB then retransmits the block using a different RV=2, and buffers the previous one. Another NACK is repeated and retransmitted for RV=3, which then soft-combines the current and buffered RVs to improve the likelihood of success, resulting in an ACK. HARQ plays a critical role in lowering the BLER in fading channels, especially in CDL scenarios with significant delay spread or Doppler effects.

2.2.2 Dynamic Scheduling

Dynamic scheduling allows for the gNB to allocate frequency-time resources adaptively to the UE on a per-slot basis. This allows for adaptation to user traffic demands, changing

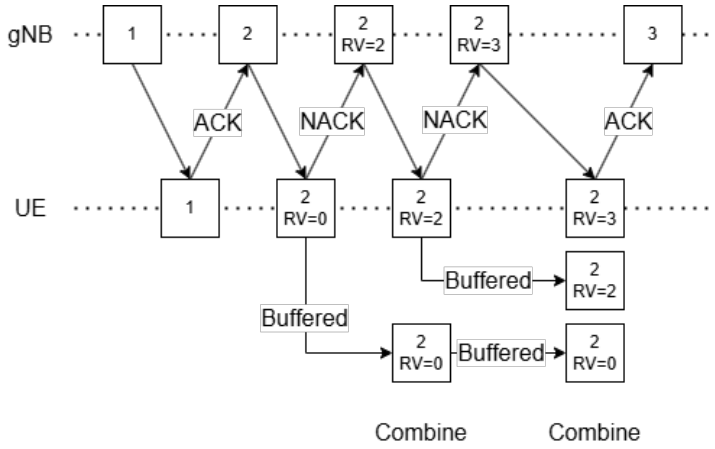

Figure 2.2: Flow of HARQ retransmission of data blocks 1, 2, and 3 with ACK and NACK examples, adapted from [13].

channel conditions, and Quality of Service (QoS) requirements. This is controlled at the PDCCH, which transmits DCI to inform the UE of the configuration of the upcoming PDSCH transmission, which includes resource allocation, MCS, and HARQ status. This is illustrated in Figure 2.3.

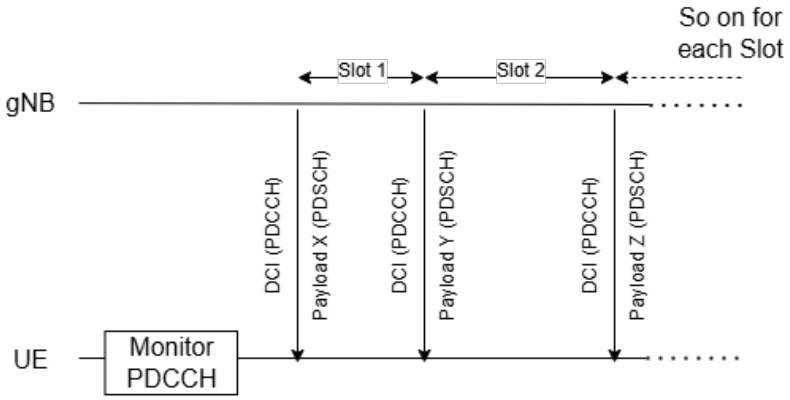

Figure 2.3: Flow of dynamic downlink scheduling, adapted from [14]. The gNB transmits a new DCI via the PDCCH in each slot, instructing the UE on how to decode the subsequent PDSCH payload. For simplicity, HARQ retransmission and Configured Scheduling (CS) are omitted.

2.2.3 Link Adaptation

Link adaptation is the process of dynamically selecting the modulation and coding scheme (MCS) based on the CQI feedback from the UE. This process enables the gNB to maximise throughput in good channel conditions by selecting a higher MCS, whilst maintaining reliability when the channel degrades by selecting more conservative ones.

A commonly used theoretical expression for throughput under link adaptation is:

$$\text{Throughput} = R \cdot \log_2(M) \cdot (1 - \text{BLER}) \tag{2.1}$$

where R is the code rate, M is the modulation order, and BLER represents the block error rate under given channel conditions.

2.2.4 Relevance to Simulation Setup

In this project, HARQ is directly implemented to reflect realistic retransmission behaviour, whilst dynamic scheduling and link adaptation are discussed here for completeness but not directly modelled. Further motives for this choice are discussed in Section 3.3.

2.3 MIMO Techniques in 5G NR

Multiple Input Multiple Output (MIMO) makes use of multiple antennas at both the transmitter (Tx) gNB and receiver (Rx) UE to send and receive multiple data streams simultaneously [12, Sec. 6.1.4]. This utilises spatial multiplexing, beamforming, and massive coverage techniques [15, Sec. 5] to significantly enhance spectral efficiency, reliability, and user throughput in different deployment spatial conditions, like dense urban and rural areas. In a typical MIMO system, the received signal vector $\mathbf{y}$ can be expressed as:

$$\mathbf{y} = \mathbf{H}\mathbf{x} + \mathbf{n} \tag{2.2}$$

where $\mathbf{x}$ is the transmitted signal vector, $\mathbf{H}$ is the channel matrix capturing the propagation between each Tx and Rx antennas, and $\mathbf{n}$ is the additive white Gaussian noise (AWGN) vector [16, Chapter 5]. The dimensions of $\mathbf{H}$ are $N_t \times N_r$, where N_t and N_r represent the number of Tx and Rx antennas, respectively.

2.3.1 Spatial Multiplexing

Spatial multiplexing allows the transmission of multiple data streams simultaneously by leveraging the spatial dimensions of the channels, independent of the time-frequency resources available [16, Chapter 7.2]. Data is organised into resource grids, in which each resource element represents the time-frequency resources defined by one sub-carrier spacing in frequency and one OFDM symbol in time [11, Sec. 7.1]. This is then mapped into layers enabling efficient parallel transmission over space, then transmitted through multiple antennas through MIMO precoding, and at the UE, uses multiple antennas to receive and decode the overlapping data streams. In 5G NR, spatial multiplexing is supported through configurations up to eight layers in the downlink, with practical implementations typically using two to four layers per user, depending on UE capabilities and demand [2, Sec 6.1.2].

Figure 2.4 illustrates the spatial multiplexing process in a Single-User (SU) MIMO system. Data streams are first mapped to transmission layers, followed by MIMO precoding before being transferred by the Tx antenna elements. The UE utilises multiple Rx antenna elements to separate and decode overlapping spatial streams.

Assuming perfect channel state information (CSI) at the Rx and given an i.i.d. Rayleigh fading channel, the theoretical capacity of such a MIMO system is given by:

$$C = \log_2 \det \left(\mathbf{I} + \frac{\rho}{N_t} \mathbf{H}\mathbf{H}^H \right) \tag{2.3}$$

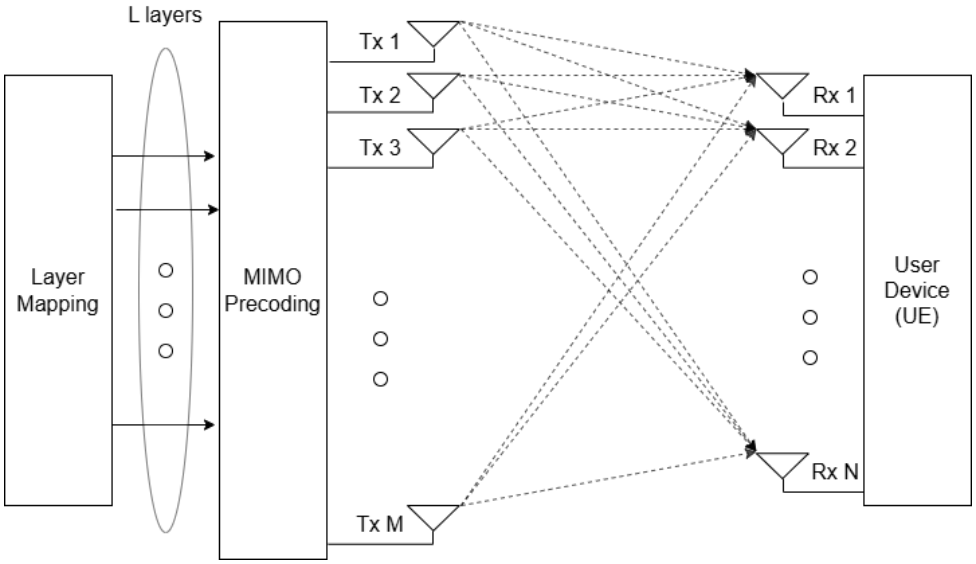

Figure 2.4: Spatial multiplexing in a Single-User (SU) MIMO system, adapted from [17].

where ρ is the average SNR at each Rx antenna, and $\mathbf{H}^H$ denotes the Hermitian transpose of the channel matrix [16, Chapter 7.3]. This expression reflects the achievable data rate improvements through spatial multiplexing under ideal channel conditions.

Whilst this capacity equation is not directly used in the project's simulation, since the MATLAB 5G toolbox evaluates throughput via link-level simulations, it is still worth noting due to its importance in providing theoretical insight into how MIMO configurations impact data rates under different channel profiles. As more layers are introduced, more simultaneous transport blocks are able to be sent, increasing the channel capacity but also increasing the sensitivity to noise and channel conditions.

2.3.2 Massive MIMO

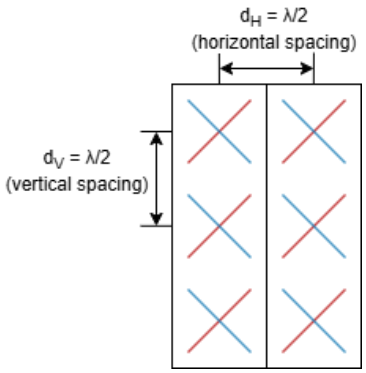

Figure 2.5: Uniform planar array consisting of two sub-arrays in a massive MIMO system, adapted from [4] and [17].

Massive MIMO combines a large number of antenna elements to provide enhanced spatial resolution, improved beamforming gain, and the ability to serve multiple users (MU-MIMO) through spatial multiplexing [15, Sec 5.2.3]. Figure 2.5 shows a simplified uniform planar antenna array consisting of two sub-arrays with 3x1 antenna elements each. These antenna elements are dual-polarised, which integrate two orthogonally polarised radiating

elements. These are typically configured with ±45°polarisation in 5G NR to minimise correlation and mutual coupling. This effectively doubles the number of usable antenna ports without requiring additional space [3, Sec. 7.3.3.2.2].

The antenna elements are grouped into sub-arrays, often in vertical columns in 5G NR, each of them are connected to an RF transmit/receive chain. This is because it would be inefficient to apply independent digital beamforming to every antenna element, due to the unnecessary need for the full range of ∓90°, as antennas are typically installed at high locations [17]. The sub-arrays are organised into a complete antenna panel, forming a uniform planar array. The element spacing is typically set to $\lambda/2$ in both vertical and horizontal directions. This is to avoid spatial aliasing and grating lobes during beam steering [3, Sec. 7.3.3.2.1]. The spatial response of such an array [3, Sec. 7.3.3.2.4] can be modelled as the direct product of the horizontal and vertical steering vectors, given by:

$$a(\theta, \phi) = a_x(\phi) \otimes a_y(\theta) \tag{2.4}$$

where $a_x(\phi)$ and $a_y(\theta)$ denote the steering vectors in the horizontal and vertical directions, respectively. This captures the 2D spatial characteristics of the antenna array and establishes a basis when forming CDL models later in Section 2.4.

Various form factors of massive MIMO are defined according to their 2D array structure. The maximum number of MIMO layers in a system is constrained to the minimum between the number of Tx and Rx antennas. In addition, [17] states that the user-specific gain is proportional to the number of sub-arrays, and the sub-array gain is approximately proportional to the number of antenna elements within a sub-array. The report also states that user-specific beamwidth is inversely proportional to the length of the massive MIMO antenna array in vertical and horizontal directions, respectively. As different deployment scenarios have different coverage needs, different-sized antenna arrays are suitable, due to the costs of implementation. For example, dense urban areas may require wider coverage, meaning a larger antenna, especially if there is high traffic demand and density with high-rise buildings, but on the other hand, for rural areas, narrow coverage is sufficient and hence a smaller antenna.

2.3.3 Beamforming

Beamforming techniques in 5G NR are designed to enable and direct signal transmission to specific users, improving SNR gains whilst nullifying interference for others [15, Sec. 5.2.3]. This is particularly valuable at higher frequencies like FR2, where path loss is severe and channel coherence is limited [3, Sec. 6.1.2.1]. Beamforming can be classified into three primary types:

- **Analogue beamforming:** Adjusts the RF signal phases across antenna sub-arrays using analogue signals; this is suitable for single-beam, high-gain transmissions
- **Digital beamforming:** Applies independent digital precoding per antenna, per user; this enables multiple simultaneous beams (MU-MIMO) through the use of null direction.
- **Hybrid beamforming:** Combines both analogue and digital domains to achieve a trade-off between hardware complexity and beamforming flexibility.

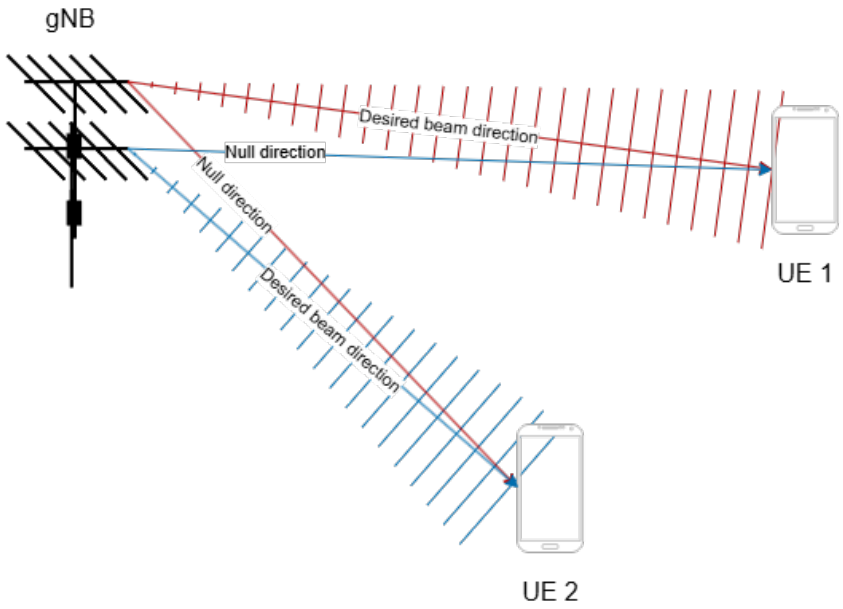

Figure 2.6: Illustration of downlink digital beamforming in a MU MIMO scenario, adapted from [17].

Figure 2.6 illustrates how digital beamforming enables MU-MIMO, where multiple users are served simultaneously with precise beams. The gNB directs narrow beams towards each UE, whilst placing nulls in undesired directions to minimise inter-user interference.

To generate such null directions, linear equalisation techniques like Zero-forcing (ZF) and minimum mean square error (MMSE) are widely studied in academic literature to mitigate inter-user interference in multi-user MIMO systems [18]. ZF precoding constructs beamforming weights by inverting the composite channel matrix, thereby creating perfect nulls in the direction of non-target users, but at the cost of amplifying noise. In MMSE, however, a balance between interference suppression and noise amplification based on SNR, ρ. The expressions for ZF and MMSE for a MIMO system are shown, respectively:

$$\mathbf{W}_{\text{ZF}} = \mathbf{H}^H(\mathbf{H}\mathbf{H}^H)^{-1} \tag{2.5}$$

$$\mathbf{W}_{\text{MMSE}} = \mathbf{H}^H(\mathbf{H}\mathbf{H}^H + \frac{1}{\rho}\mathbf{I})^{-1} \tag{2.6}$$

Whilst both methods provide valuable theoretical insights, they are not specified in the 3GPP 5G NR standards. In practice, 5G downlink systems are reliant on codebook-based precoding, where the UE returns a precoding matrix indicator (PMI) from a standardised codebook. Using this PMI, the gNB selects precoding vectors from the codebook to minimise spatial overlap and approximate interference [2, Sec. 5.1]. However, once the gNB receives the feedback, vendors may integrate their custom channel estimation and equalisation filters, provided they align with the codebook-based precoding structure [2, Sec. 6.1.3], hence noting the importance of ZF and MMSE here.

2.3.4 CSI Reporting and Precoding

In 5G NR closed-loop MIMO, Channel State Information (CSI) feedback enables the gNB to adapt its transmission scheme to current channel conditions. CSI is acquired at the UE

based on observation of downlink reference signals (RS), which are fed back to the gNB through different quantised indicators. These indicators include Rank Indicator (RI), Precoding Matrix Indicator (PMI), and Channel Quality Indicator, as specified in 3GPP TS 38.214 [2, Sec. 5.2 and 6.1.3.1].

The Rank Indicator (RI) denotes the number of spatial layers, i.e. parallel data streams, that the UE deems suitable for reliable transmission based on the current channel conditions. A higher RI suggests better spatial separability between the Tx-Rx antenna, usually achievable in high-scattering or high-SNR environments.

The Precoding Matrix Indicator (PMI) denotes the preferred precoding matrix index from a standardised codebook defined by 3GPP TS 38.214 [2, Sec. 5.2.2.2]. Based on the observation of reference signals from CSI-RS, the UE evaluates the matrix which maximises metrics like SNR, throughput, or mutual information. Type-1 codebooks are commonly used for SU-MIMO, whereas Type-2 codebooks are used for MU-MIMO, and both support wideband or subband PMI reporting suitable up to 8 MIMO layers.

The Channel Quality Indicator (CQI) denotes the optimal modulation and coding scheme (MCS) that could support a target block error rate (BLER) based on MCS tables defined in 3GPP TS 38.214 [2, Sec. 5.1.3.1]. Again, this is based on the observations of effective SNR or mutual information. This is the link adaptation feature discussed in Section 2.2.3 to maximise throughput depending on channel conditions.

CSI acquisition in 5G NR is based on the transmission of CSI-RS, which are mapped reference symbols used by the UE for channel estimation. These symbols are configured to cover time, frequency, and spatial characteristics of the channel. Perfect CSI reporting assumes that the gNB has direct access to the full channel matrix, $\mathbf{H}$, without quantisation or delay [16, Chapter 7.6]. However, realistic CSI reporting is constrained by quantisation, feedback periodicity, and processing delays. This results in imperfect CSI being reported at the transmitter, leading to precoding mismatches and hence, reduced system performance. Comparing these two scenarios helps to evaluate the performance gap introduced by imperfect CSI reporting and to understand trade-offs in precoding accuracy and system throughput.

2.3.5 Channel Estimation

Channel estimation allows the UE to obtain an estimate of the channel matrix, $\hat{\mathbf{H}}$, used for equalisation, demodulation, and decoding, based on known Demodulation Reference Signal (DM-RS). DM-RS are pilot symbols transmitted with the PDSCH, which are known a priori to the UE, allowing it to isolate the channel conditions from the received signals. Depending on the configuration, DM-RS can span multiple OFDM symbols and subcarriers, with mapping type A or B defined in 3GPP TS 38.214 [8, Sec. 6.4.1.1.3]. This influences the granularity and quality of channel estimates, especially in high Doppler environments.

The process of estimating the channel from these pilots can be vendor-specific, carried out in a variety of techniques. The simplest and computationally efficient approach is the Least Squares estimator, directly solving for minimal squared error between the received

and known pilot symbols. This, however, is invariant to noise. Other approaches, like Minimum Mean Square Error (MMSE) [18], are employed to tackle these issues. MMSE takes into account second-order statistics, i.e. channel and noise covariance, to optimally balance noise suppression, albeit at the cost of higher computational complexity. This estimation is then followed by equalisation, such as Zero Forcing (ZF) and MMSE equalisation, to effectively remove any inter-layer interference.

Perfect channel estimation is where the receiver is assumed to have full knowledge of the true channel matrix, $\mathbf{H}$, whereas with realistic estimation, pilot-based algorithms like least squares or MMSE are used under channel noise and distortion. Comparing the performance between perfect and imperfect channel estimation helps to evaluate the upper bound on receiver performance, but also helps to accurately capture the degradation in practical channel conditions.

2.3.6 Relevance to Simulation Setup

This project focuses on investigating the performance of the PDSCH under varying channel models and antenna configurations using CDL profiles. Within the end-to-end 5G NR system, MIMO configurations are simulated in SU-MIMO scenarios not only to simplify simulation steps but also to align results with current industry developments. Whilst some companies have explored MU-MIMO configurations, the majority of recent evaluation efforts, particularly those discussed during the 3GPP RAN4 #114 meeting seen in Table B.1, continue to focus on SU-MIMO configurations due to their standardisation relevance, better reproducibility, and clearer benchmarking against channel model behaviour. Imperfect CSI feedback along with imperfect channel estimation is also implemented into the simulations to better reflect practical deployments, and the performance trade-offs between ideal and realistic scenarios are evaluated.

2.4 Wireless Channel Modelling

Accurate wireless channel modelling is essential for evaluating the performance of 5G NR systems. Channel models capture key features of an environment, such as fading, path loss, and Doppler effects [3, TR 38.901, Sec. 6]. This section provides a comprehensive overview of the primary modelling approaches used in 3GPP.

2.4.1 TDL and CDL Models: Definitions and Use Cases

The Tapped Delay Line (TDL) and Clustered Delay Line (CDL) models represent two classes of stochastic geometry-based channel models:

TDL Models

TDL models are characterised by a discrete set of multipath components, known as a 'tap', each with a fixed delay and a fading process in the time domain. This is defined by a power delay profile, which assumes all multipath components arrive with zero angular dispersion. This means no spatial characteristics, which includes angles of arrival or departure [3, Sec. 7.7.2].

Equation 2.7 expresses the wireless channel as a sum of multiple delayed and scaled versions of the transmitted signal:

$$h(t,\tau) = \sum_{l=1}^{L} h_l(t)\delta(\tau - \tau_l) \tag{2.7}$$

- L: Number of taps
- $h(t,\tau)$: Time-varying complex gain for tap l
- τ_l: Delay of tap l

TDL models are useful for single-antenna evaluations and statistical fading studies without spatial structure. Typically used in link-level simulations without explicit antenna array geometry involved, and is suitable for modelling rural areas without many scatterers.

CDL Models

CDL models extend the concept of TDLs by grouping multipath components into clusters, each with a defined angular spread in both azimuth and elevation, to model spatial characteristics for the Tx and Rx antenna. Each cluster is composed of multiple rays, capturing Angle of Departure (AoD), Angle of Arrival (AoA), Doppler shifts, and delay spread [3, TR 38.901, Sec. 7.7.1]. The MIMO channel impulse response in a CDL model is defined in Equation 2.8:

$$\mathbf{H}(t,\tau) = \sum_{n=1}^{N} \sqrt{P_n}\mathbf{a}_r(\phi_n^{\text{AoA}}, \theta_n^{\text{AoA}})\mathbf{a}_t(\phi_n^{\text{AoD}}, \theta_n^{\text{AoD}})e^{j2\pi f_{D,n}t}\delta(\tau - \tau_n) \tag{2.8}$$

- N: Number of rays
- a_t, a_r: Transmit and receive array steering vectors defined in Section 2.3.2
- ϕ, θ: Azimuth and elevation angles
- $f_{D,n}t$: Doppler shift
- P_n Power of ray n

CDL models are specifically designed for multi-antenna evaluations through their spatial characteristics, enabling their use in evaluating MIMO techniques, beamforming, and spatial correlation effects, especially in dense urban and suburban areas.

Comparison of TDL and CDL models

Figure 2.7 shows the comparison between TDL and CDL channel model paths. In the TDL model, multipath components are modelled as discrete taps with a fixed delay profile and average power with no angular information. The multipath components consist of the direct, reflected, and diffracted wave paths of the signal. In contrast, the CDL model groups rays into spatial clusters, each characterised by a common delay profile and a distribution of AoA and AoD.
A single ray from each cluster is shown with its respective angles in Figure 2.7. Note that cluster 2 is labelled as 'NLOS', which stands for Non-Line-of-Sight, as opposed to the other clusters 1 and 3, which are Line-of-Sight (LOS). LOS rays refer to the direct transmission path between the Tx and Rx, whilst NLOS rays involve only reflected, scattering, and diffracted paths [3, Sec. 7.51]. This results in NLOS typically having weaker and more

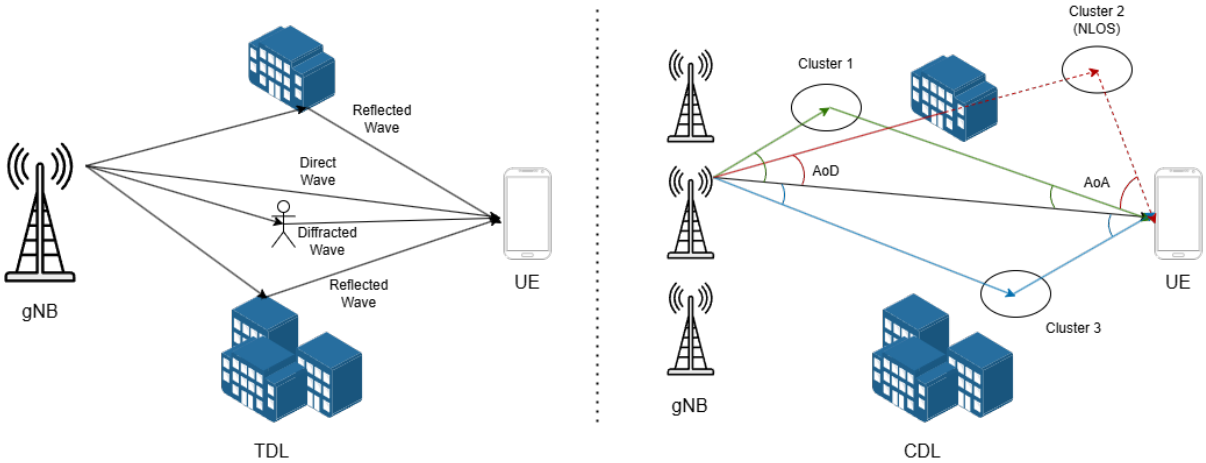

Figure 2.7: Illustration of TDL (left) vs. CDL (right) channel model paths, adapted from [14] and [19]

dispersed signals, but they provide more realistic evaluations of most indoor and outdoor environments.

Since TDL models have no angular modelling, no spatial correlations, and fewer rays to evaluate, they have lower computational complexity costs than CDL models. However, CDL models will provide a more accurate and realistic simulation for MIMO.

2.4.2 CDL Model Profiles in 3GPP

To support different urban contexts, 3GPP defines five CDL profiles, labelled CDL-A through CDL-E, in [3, TR 38.901, Tables 7.7.1-1-5]. Each of these models represents typical propagation scenarios ranging from NLOS to LOS, microcell to macrocell urban environments. The tables for each CDL model in [3] consist of a fixed number of clusters, with specific delays, power, AoA, and AoD.

Table 2.1 summarises each of the CDL profiles, highlighting their key differences in environment type, LOS conditions, typical use cases and deriving their respective RMS delay spreads, computed using the standard second-moment formula:

$$\tau_{\text{RMS}} = \sqrt{\sum_i P_i(\tau_i - \tilde{\tau})^2}, \quad \text{where } \tilde{\tau} = \sum_i P_i \tau_i \tag{2.9}$$

Here, P_i and τ_i denotes the power and delay of multipath component i respectively.

Note that all CDL profiles defined are designed towards an urban environment. This is because rural areas contain fewer scatterers, meaning that direct propagation paths are typically longer, and it would be of best interest in computational and integration costs to implement TDL models. [20] evaluates the effectiveness of CDL model implementation in rural areas, which will be discussed further in Section 2.5.1.

2.4.3 Relevance to Simulation Setup

Using standardised CDL models in the simulation setup, defined in 3GPP [3, TR 38.901, Tables 7.7.1-1-5], ensures the reliability and consistency of any analysis of results given,

Model	Environment	LOS/NLOS	Delay Spread	Use Case
CDL-A	Urban Microcell (UMi)	NLOS	Low (30 ns)	Low-scattering, short-range links
CDL-B	Urban Microcell (UMi)	NLOS	High (300 ns)	Rich multipath, low antenna correlation
CDL-C	Urban Macrocell (UMa)	NLOS	High (300 ns)	Dense urban NLOS, spatial diversity
CDL-D	Urban Macrocell (UMa)	LOS	Moderate (100 ns)	LOS with moderate reflection
CDL-E	Urban Macrocell (UMa)	LOS	Moderate (100 ns)	Strong LOS, directional channels

Table 2.1: Summary of standard CDL channel profiles defined in [3, TR 38.901, Tables 7.7.1-1-5]

concerning real-life deployment scenarios. This provides strong arguments for certain trends and sensitivities in data, ensuring practical relevance.

2.5 Simulation-Based Studies in Literature

This section reviews academic studies that have adopted similar simulation frameworks to investigate physical layer performance using CDL channel models, particularly work that is closely relevant to this project. By exploring each study individually, we aim to highlight the objectives, methodologies, assumptions, and performance results, as well as identify any gaps or limitations that further support our simulation approach discussed in Section 3.

2.5.1 Use of Standardised Channel Models

Mohamed [21] focuses on the impact of waveform parameters, specifically numerology, on PDSCH throughput under both TDL-C and CDL-C models. TDL-C is also a 3GPP-defined profile like CDL-C in [3, TR 38.901, Table 7.7.2-3]. This study is primarily concerned with subcarrier spacing, i.e. bandwidth, and highlights how throughput trends vary significantly depending on the channel model used. The author concludes that the throughput for the CDL-C model remains stable for small numerologies compared to the TDL-C model, especially at high bandwidths. This is linked to the spatial correlation that CDL provide over TDL models. Whilst this study does not delve deeply into spatially correlated behaviour, it underlines the importance of selecting a realistic channel model when evaluating downlink system performance.

Pessoa et al. [20], on the other hand, propose a CDL-based channel model tailored for 5G MIMO systems operating in rural and remote areas, with a particular emphasis on dual-polarised antenna elements as opposed to single-polarised ones. This study derives its CDL model based on standardised 3GPP CDL-A and CDL-D models and incorporates relevant rural propagation parameters, such as larger cell radii and reduced scatterer density. The authors note that scenarios with limited scattering often lead to channels with lower ranks, affecting the performance of MIMO systems. Whilst the study does not focus on link-layer performance metrics like throughput or BLER, and focuses more on channel-level metrics like angular spread and eigenvalue distribution, it contributes to literature by demonstrating what CDL models can achieve in remote rural areas beyond the urban macro/micro capabilities defined in Table 2.1. This study emphasises the flexibility of CDL models and their applicability to a broader range of 5G use cases, supporting the choice of 3GPP-defined CDL models in this project.

2.5.2 Throughput Evaluation under CDL

Baghous [22] conducts a comprehensive performance evaluation of 5G NR downlink system throughput between massive MIMO and MIMO under NLOS CDL models, namely CDL-A/B/C. This study varies antenna array sizes independently for the Tx and Rx side, and concluded that there is an evident increase in performance in lower SNRs when increasing the number of Tx antennas, but when increasing the number of Rx antennas, a performance increase between MIMO and massive MIMO systems. Whilst the study references 3GPP-defined CDL profiles, it does not align its simulation with standardised physical layer procedures as defined in 3GPP TS 38.214 [2]. Nonetheless, this study highlights the sensitivity of throughput in different CDL NLOS profiles, emphasising the importance of evaluating performance-based metrics like throughput.

2.5.3 Gaps in Methodology and Realism

Almahadeen and Martarneh [23] present a performance assessment of 5G system throughput by examining the influence of different subcarrier spacing (SCS), modulation schemes, and the use of reflectors within the FR1 channel environment. Whilst the study does not reference the use of standardised 3GPP channel parameters and specify the exact CDL model used, the simulation structure and terminology suggest a likely use of MATLAB's 5G Toolbox with the default parameter setting. The authors conclude that performance, i.e. throughput, decreases proportionally with SCS, with 15, 30, 60, and 120 kHz producing 12%, 40%, 68.25%, and 100% throughput, respectively, at 0 dB. They also demonstrate that higher-order modulation schemes produce higher throughput, but also make use of reflectors to demonstrate the properties of CDL models and how the position of the reflector affects throughput. However, the paper lacks clarity regarding the simulation setup, including channel model assumptions, and provides minimal interpretation of the presented results. Nevertheless, this study reinforces the wider importance of 5G NR physical layer tuning, offering conceptual relevance to this project's more standardised simulation approach.

2.5.4 Summary and Motivation

In summary, the reviewed simulation-based academic studies provide valuable insights into the performance evaluation of 5G NR downlink systems. However, it is evident that there are several limitations within these studies, such as the use of non-standardised 3GPP parameters and the minimal discussion on the role of HARQ. This project aims to build upon the existing work by rigorously implementing standardised configurations and making comparisons with ongoing Industry development results.

2.6 Industry Reports and Standardised Parameters

In recent industry developments, the 3GPP RAN4 group has been advancing the demodulation performance requirements of CDL models through standardised PDSCH simulations under the agenda item, 7.16.2 Spatial channel modelling methodology, in the #114 and #115 meeting report [6], [24]. This initiative is tied to the upcoming technical report TR 38.753 [25] associated with Release 19 of the 3GPP specification. This agenda item aims to develop CDL models, revising the baseline models defined in TR 38.901 [3], to

better reflect realistic demodulation scenarios and deployment conditions, like Doppler, antenna position and azimuth. As developments towards this item are still currently ongoing, the channel parameters are still under revision with each new meeting and way forward. Hence, as access to the current revision of the 38.753 [25] CDL model is currently limited and subject to change at any point, this project aims to replicate simulations using the same channel parameters but instead by using the baseline 38.901 [3] CDL model to offer critical opinions on the changes so far.

2.6.1 Standardised Parameters

As of 3GPP RAN4 #115 meeting, Table 2.2 shows the simplified approved parameters to simulate demodulation performance. The full parameter list is shown in Appendix B in Table B.2.

Parameter		**Value**
FR / Carrier frequency		FR1, 3.5 GHz
Doppler shift/UE speed		10 Hz, 100 Hz or 3 km/h, 30 km/h
Antenna configuration		Rank 4: 4Tx, 4Rx Rank 8: 8Tx, 8Rx
Number of layers		8, 4
PMI		Random, Fixed
Waveform		CP-OFDM with normal CP
Channel Bandwidth/SCS		40 MHz / 30 kHz
MCS		13 (64 QAM table)
PDSCH configuration	Mapping type	Type A
	Length (L)	12
NZP CSI-RS for CSI acquisition	CSI-RS resource type	Aperiodic
	Number of CSI-RS ports (X)	4 CSI-RS Ports (2, 1) for 4 Layer 8 CSI-RS Ports (4, 1) for 8 Layer
Number of HARQ processes		8
Maximum HARQ transmissions		4

Table 2.2: Simplified standardised parameter table for PDSCH performance under SU-MIMO (FR1) from TDoc R4-2504616 [26]. Table of full parameters in Appendix B.

Channel Models:

- UMa-CDL-C A1: CDL (TR 38.753) with Table 7.2.1-8 in TR 38.827
- UMa-CDL-C A2: CDL (TR 38.753) based on untruncated CDL-C from Table 7.2.1-3 in TR 38.901
- UMa-CDL-C A3: CDL (TR 38.753) based on truncated CDL-C from Table 7.2.1-3 in TR 38.901

Antenna Array Vector (AAV) Configuration:

- Option 1: with AAV with subarray configuration
  - (M, N, P, M_s, N_s) = (8, 8, 2, 8, 4) for 8Tx CSI-RS Ports (Option X)
  - (M, N, P, M_s, N_s) = (8, 8, 2, 8, 2) for 8Tx CSI-RS Ports (Option X)
  - (M, N, P, M_s, N_s) = (8, 4, 2, 8, 1) for 8Tx CSI-RS Ports (Option Y)
  - (M, N, P, M_s, N_s) = (8, 2, 2, 8, 1) for 4Tx CSI-RS Ports (Option Y)
- Option 2: with AAV without subarray configuration
  - (M, N, P, M_s, N_s) = (8, 8, 2, 8, 8) for 8Tx and 4Tx CSI-RS Ports
- Option 3: with AAV configuration

- (M, N, P, M_s, N_s) = (1, 4, 2, 1, 1) for 8Tx CSI-RS Ports
- (M, N, P, M_s, N_s) = (1, 2, 2, 1, 1) for 4Tx CSI-RS Ports

where M and N is the number of antenna elements in the vertical and horizontal direction, respectively, P is the polarisation, i.e. dual-polarisation, M_s and N_s are the number of elements per subarray in the vertical and horizontal direction, respectively.

These simulations are done in FR1, 3.5 GHz, with channel bandwidth 40 MHz, tested under Doppler, 10 Hz or 100 Hz, and under MIMO layers supporting up to 8 layers. We observe that the MCS is fixed at 64 QAM. This means there is no link adaptation involved as discussed in Section 2.2.3. We also observe that HARQ reprocessing is simulated alongside Non-Zero Power (NZP) CSI-RS, which means non-ideal CSI is estimated [11, p. 7.4.1.5].

Looking at the AAV configurations, option one models large antenna arrays, option 2 serves as a baseline without subarrays, and option three models compact antenna arrays. The current shift of focus for the 3GPP RAN4 group currently lies in simulating option 1Y and option three as of #115 meeting report [24]. As part of the project scope, which aims to evaluate the performance between MIMO configurations (i.e., layers) and Doppler within a practical setting, option three is mainly used for simplicity, and option 1Y implementation is briefly investigated.

2.6.2 Full Throughput Curves of Industry Simulation Results

TDoc R4-2502377 [27] and TDoc 45-2507823 [28] contain the simulation results and alignment of different companies attributed to the 3GPP development from the RAN4 #113 and #115 meeting, respectively. In Appendix B, Table B.1 summarises the list of Tdocs containing the simulation results from each of the different companies. Figure 2.8 shows the industry throughput against SNR alignment curves for option 1Y, 8Tx/4Rx 4-layer 10 Hz and 100 Hz cases and the 8-layer 10 Hz case. We note that the results shown are as of the RAN4 #113 Meeting, in which the two Doppler cases results are investigated, hence the reason for the lack of companies shown. These results, in particular, were chosen to emphasise the impact of Doppler shifts of 10 Hz and 100 Hz, which correspond to UE speeds of 3 km/h and 30 km/h, respectively, which simulate pedestrian walking and slow urban driving or cycling.

We observe that for the 4-layer cases in Figure 2.8a and b, relative throughput increases as the channel is exposed to higher SNRs. The change in Doppler shifts from 10 Hz to 100 Hz only leads to a performance loss of around 0.5 dB. This is unexpected as Pawase and Chang [29] suggest that significant Doppler shifts lead to rapid channel variations, in which a standard DM-RS cannot keep up, leading to a larger number of decoding errors, hence less throughput. This is mainly due to vendors implementing their own channel estimation techniques, especially ones with temporal considerations. Kim et al. [30] highlights the impact and importance of Kalman filtering and machine learning algorithms for temporal channel estimation. As discussed in Section 2.3.5, the process of estimating the channel is vendor-specific. Although each vendor's implementation is not publicly reported, we can assume that each vendor takes mobility effects into consideration, hence the small performance loss.

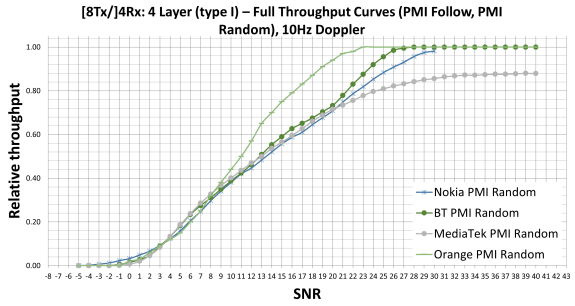

(a) 8Tx/4Rx, 4 Layer, 10Hz Doppler

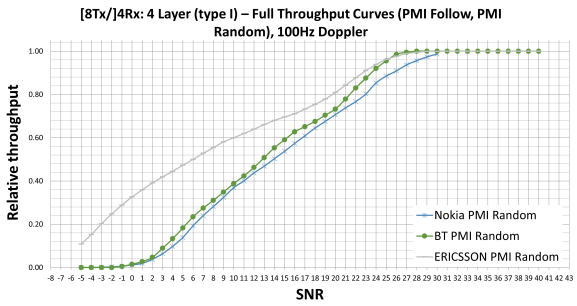

(b) 8Tx/4Rx, 4 Layer, 100Hz Doppler

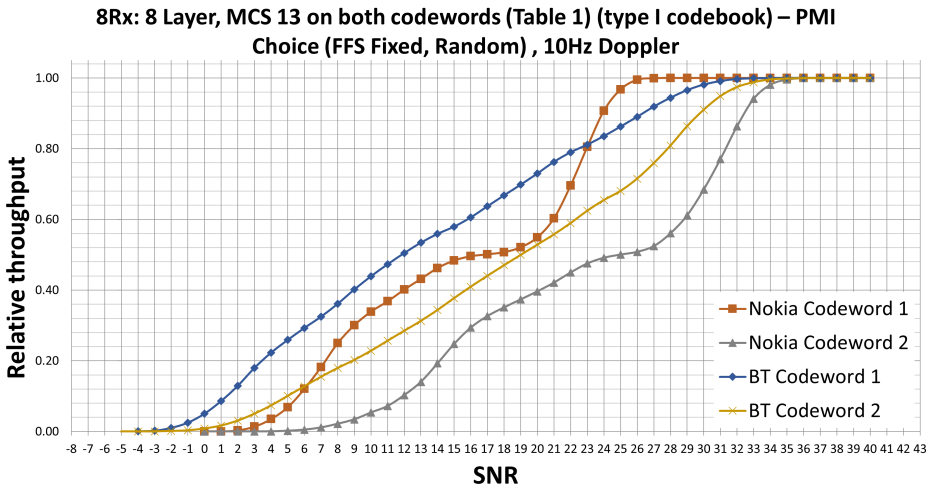

(c) 8Tx/8Rx, 8 Layer, 10Hz Doppler

Figure 2.8: Full throughput curves of industry simulation results alignment for AVV Option 1Y, from #113 meeting TDoc R4-2502377 [27].

Nokia and BT results seem to align closely, but for MediaTek, Orange, and Ericsson, all perform differently. It is worth noting that since these results are from earlier versions and meetings, a fully standardised simulation configuration may not have been put forward. As a result, vendors like Ericsson may have increased performance due to better CSI, PMI, or channel estimation implementation. For example, if we look at the 8-layer case in Figure 2.8c, a double "dipping" effect is observed in Nokia's results as opposed to BT's curves. This effect is caused by HARQ retransmissions, which lead to temporary reductions in throughput, especially in mid-SNR regions, as Alsharbaty and Fasola [31] conclude in their HARQ analysis on the performance of LTE systems. From this, we can infer that BT has not enabled HARQ retransmissions in their simulations and that at the time of this alignment, a standardised simulation procedure has not been established.

The Tables 2.3 2.4, and 2.5 summarise the option three results for 4-layer and 8-layer cases with CDL option 1 and 2 models at 30% and 70% throughput, as of RAN4 #115 meeting. CDL-C option one is based on the draft TR 38.753 with different angular and delay spreads than the 38.901 model. CDL-C option two is based on the untruncated TS 38.901 model with new features like ray splitting [32, Issue 4-1-6]. We observe that the span of results for the 4-layer case is closely in line, as opposed to the 8-layer case, where the span ranges widely between vendors. There still seems to be disagreement with simulation configurations as of the latest meeting. By reproducing the industry

simulations, following closely with standardised parameters set by 3GPP, and carefully evaluating the steps we take, it might be worthwhile comparing the simulation results with the industry-reported results to offer any key insights as to why some vendors may have differing results.

Channel Model AAV Option 3	Throughput (%)	Apple	BT	Ericsson	Huawei	MTK	Nokia	Qualcomm	Samsung	ZTE	Span	Average
CDL Option 1	30	8.1	8.2	6.4	6.3	6.1	7.1	5.7	6.9	8.6	2.9	7.0
	70	15.3	16.0	16.5	15.7	16.5	18.0	13.4	15.6	17.3	4.6	16.0
CDL Option 2	30	8.8	6.3	6.36	6.6	6.4	7	6.1	7		2.7	6.8
	70	15.2	14.9	16.48	15.6	15.9	16.6	15.1	15.7		1.7	15.7

Table 2.3: Summary alignment across vendors for 4x4, 4 Layer

Channel Model AAV Option 3	Throughput (%)	BT	Ericsson	Huawei	MTK	Nokia	Qualcomm	Span	Average
CDL Option 1	30	6.8	4.9	5.5	5.6	6.4	21.5	16.6	8.5
	70	16.6	14.2	18.2	17.0	17.1	23.0	8.8	17.7
CDL Option 2	30	5.4	4.9	4.8	6.1	6.8	10.7	5.9	6.5
	70	17.9	14.2	16.5	16.7	17.5	21.4	7.2	17.4

Table 2.4: Summary alignment across vendors for 8x8, 8 Layer, Codeword 1

Channel Model AAV Option 3	Throughput (%)	BT	Ericsson	Huawei	MTK	Nokia	Qualcomm	Span	Average
CDL Option 1	30	9.6	15.7	9.4	9.7	11.9	22.5	13.1	13.1
	70	20.3	26.5	26.8	24.3	24.6	28.0	7.7	25.1
CDL Option 2	30	13.3	15.7	10	9.9	11.6	14.3	5.8	12.5
	70	26.3	26	24.4	24	24.7	35.3	11.3	26.8

Table 2.5: Summary alignment across vendors for 8x8, 8 Layer, Codeword 2

2.7 Summary and Research Motivation

This chapter has outlined the fundamental concepts underpinning 5G NR downlink performance, with a focus on MIMO systems, CSI feedback mechanisms, and standardised channel modelling CDL models defined in 3GPP TS 38.901 [3]. A review of the literature and industry documentation has highlighted the evident gaps in academia.

Several key insights emerged from this review. First, although academic journals do use 3GPP-defined procedures and models, they often make ideal assumptions, such as no HARQ or perfect CSI, to benchmark certain parameters or features [20], [22]. However, these ideal assumptions mask many of the trade-offs and limitations encountered in practical deployments. Industry interests have shifted toward more realistic evaluations.

Second, whilst the 3GPP standards define CSI reporting structures and channel model templates, vendors often adopt proprietary implementations that introduce notable discrepancies in reported performance results. These differences can arise from estimation methods, codebook selection strategies, or assumptions around feedback latency.

This study is therefore motivated by the need to bridge the gap between standard-aligned theoretical models and the vendor-specific realities of implementation. By employing MATLAB's 5G Toolbox to construct a controlled yet flexible simulation framework, this dissertation aims to analyse how feedback imperfections, estimator design, and array structure affect system throughput. The next chapter details the methodology used to conduct these evaluations and justify the choices made in the simulation configuration.

3. Methodology

3.1 Overview of Simulation Environment and Workflow

The simulation environment is implemented using MATLAB's 5G Toolbox [7] and the Phased Array System Toolbox [33]. This environment follows an end-to-end structure that accurately models the physical layer of a 5G NR downlink transmission with features such as channel models, CSI feedback, HARQ, and channel estimation. The workflow is designed to reflect the 3GPP standard-compliant procedures defined in TS 38.211, TS 38.212, and TS 38.214 [2], [8], [9]. A block-level representation of the transmitter, channel, and receiver chain is shown in Figure 3.1.

This choice of MATLAB aligns with a wide body of academic and industry research (e.g. Baghous [22], Pessoa et al. [20], and Zhang et al. [34]), where MATLAB-based link-level simulations are commonly employed to evaluate physical-layer performance in 5G and beyond. Moreover, the high-level abstraction and integrated visualisation tools in MATLAB facilitate rapid iterations across parameter sweeps, making it ideal for performance benchmarking, especially under realistic end-to-end simulations.

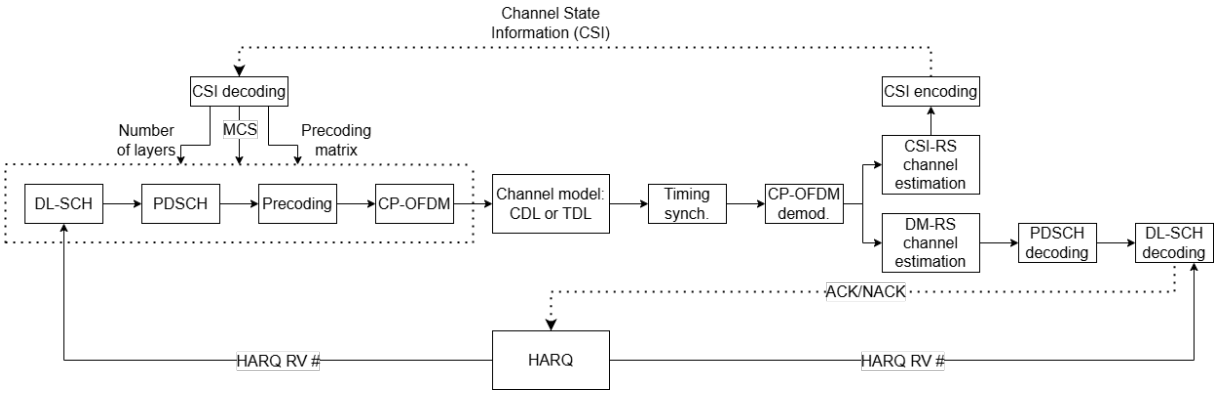

Figure 3.1: Flow diagram of the implemented end-to-end processing chain for a 5G NR downlink system. Adapted from the MATLAB 5G Toolbox [7].

On the transmitter side, the process begins with DL-SCH encoding, followed by PDSCH processing, precoding dependent on the configured MIMO scheme, and then Cyclic Prefix (CP)-OFDM modulation. The waveform is passed through a propagation channel model implemented using the `nrTDLChannel` and `nrCDLChannel` object functions from the 5G Toolbox to model TDL and CDL channel models. This object allows for a flexible configuration, which will be further discussed in Section 3.2. These models enable realistic simulation of multi-path channels in line with industry practice.

At the receiver side, timing synchronisation and CP-OFDM demodulation are followed by channel estimation using both DM-RS and CSI-RS, discussed in Sections 2.3.4 and 2.3.5, dependent on the current channel conditions. Using the reference signals to acquire CSI, this is then used to perform PDSCH and DL-SCH decoding to recover the transmitted data. CSI feedback is generated through the estimation of different quantised indicators, such as RI, PMI, and CQI, which are configured to be ideal or non-ideal depending on the

chosen configuration. This information is sent back to the transmitter, where the MCS, number of layers, and precoding matrix are adaptively selected based on maximum performance. All CSI indicators are implemented in the simulation and tested. Specifically, the number of layers and MCS are fixed, and a codebook type-1 based PMI is used to align with industry data.

HARQ, discussed in Section 2.2, is also integrated through a feedback loop. When decoding fails, a NACK is generated and the corresponding RV is tracked and updated to the {0, 2, 3, 1} sequence. The HARQ buffer is soft-combined across retransmissions for incremental decoding gains. HARQ plays a critical role in lowering the BLER in fading channels, especially in CDL scenarios with significant delay spread or Doppler effects, reflecting error recovery.

This simulation framework is highly configurable, supporting studies of various physical-layer features such as CSI reporting, HARQ retransmissions, UE mobility (Doppler), and MIMO layer scaling through the use of the 5G Toolbox as well as its inbuilt helper functions.

3.2 CDL Architecture

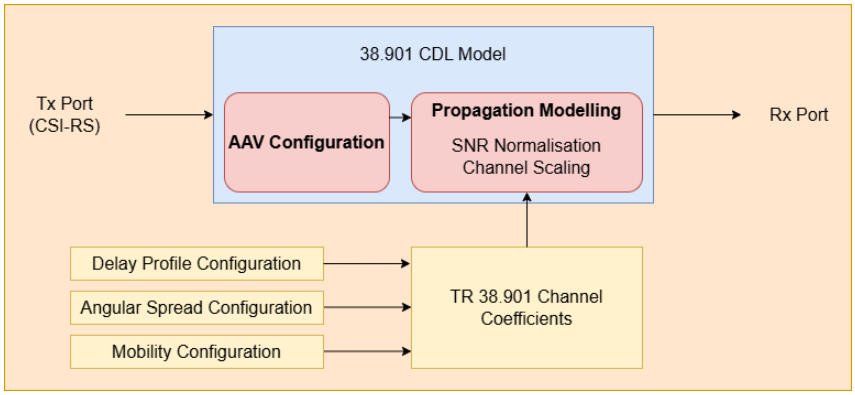

Figure 3.2: Internal architecture of the 38.901 CDL model, adapted from MATLAB 5G Toolbox [7] and TR 38.901 [3, Sec. 7.7.1].

Figure 3.2 illustrates the internal architecture and configuration flow of the 3GPP TR 38.901 CDL model [3, Sec. 7.7.1], implemented via the `nrCDLChannel` object in MATLAB's 5G Toolbox. This architecture comprises two main processing components: Antenna Array and Virtualisation (AAV), and propagation modelling.

AAV determines how signals are transmitted and received across multi-element antenna arrays. This is configured in the `TransmitAntennaArray` and `ReceiveAntennaArray` properties of the `nrCDLChannel` object. This allows the array dimensions, element spacing, polarisation angles, orientation, and element type to be configured at both the gNB and UE antennas.

The propagation modelling block allows fading and channel scaling effects to be configured. The delay profile, i.e. CDL model profiles, selects a predefined power-delay profile from TR 38.901 [3, Section 7.7.1]. The azimuth and elevation spreads can also be configured along with the user mobility. These parameters influence the generated channel

impulse response, which then can be passed through the receiver's channel estimation routines.

3.3 Configuration Parameters

The following configuration parameters are used for the final end-to-end downlink 5G NR implementation. This includes features like DM-RS, CSI feedback, and HARQ, in which the performance of these features is evaluated in comparison with and without them. These parameters were chosen based on the industry testing parameters listed in Appendix B and 3GPP specifications.

Parameter		**Value**
Carrier Frequency		FR1, 3.5 GHz
Size of Bandwdith		52 PRB
Channel Bandwidth/SCS		40 MHz / 30 kHz
Channel Model		CDL-A/B/C/D/E
Doppler Shift		10 Hz, 100 Hz
MIMO layers and Antenna Configuration		2 Layer: 4Tx, 4Rx 4 Layer: 8Tx, 4Rx 8 Layer: 8Tx, 8Rx
Waveform		CP-OFDM with normal CP
MCS		Fixed: 13 (64 QAM table)
SNR Range		-5 to 25 dB
PDSCH Configuration	Mapping Type	A
	Starting Symbol	2
	Length	12
DM-RS Configuration	Type	1
	Additional Position	1
	Length	Rank 4: 1 Rank 8: 2
CSI Feedback (Aperiodic)	PMI	Random: Subband every PRB Bundle (size = 2)
	Subband Size	4 PRB
	Number of Subbands	13
	Codebook Type	Single Panel Type I
	Number of CSI-RS ports	4 Layer: 4 CSI-RS Ports (2, 1) 8 Layer: 8 CSI-RS Ports (4, 1)
	CSI-RS Row Number	Rank 4: 4 Rank 8: 6
	Periodicity	Every 5 slots
	Symbol Locations	13
	Subcarrier Locations	Rank 4: 0Rank 8: [0, 3, 6, 9]
	Density	1
LDPC Configuration	Algorithm	Layered Belief Propagation
	Maximum Iteration Count	6
HARQ Configuration	Number of HARQ processes	8
	Maximum number of HARQ transmissions	4
	RV sequence	{0,2,3,1}
AAV Configuration	UE Size	4Rx: [2 1 2 1 1] 8Rx: [2 2 2 1 1]
	gNB Size	4Tx: [1 4 2 1 1] 8Tx: [1 2 2 1 1]
	UE Element Spacing	[0.5 0.5 1 1]
	gNB Element Spacing	[0.5 0.5 4 1]
	LCS UE	[180, 0, 0]
	LCS gNB	[0, 10, 0]
	UE polarisation and pattern	(0, +90), isotropic
	gNB polarisation and pattern	(-45, +45), 38.901

Table 3.1: Final simulation configuration parameters used for evaluating SU-MIMO performance

SU-MIMO was implemented for simplicity and to align with current industry-reported simulations, and MU-MIMO can be implemented easily using the `nrCDLChannel` object for future work. Transmission features, discussed in Section 2.2, and a least squares channel estimator are systematically implemented with suitable tests and validation with reviewed

literature, using the initial configuration of 8Tx/4Rx 4-layer with AAV option 3, CDL-C, delay spread of 300 ns and Doppler shift of 10 Hz. A least squares channel estimator is used due to its ease of implementation, low computation complexity, and to provide groundwork for future improvements. After a suitable simulation environment is built and validated, the use of different CDL models discussed in Section 2.4.2, different Doppler shifts, and MIMO configuration is evaluated through performance metrics like throughput and BLER. These results are then compared with existing literature and industry reports to provide key insights, aiming to close the gap between academic and industry work.

3.4 Subarray Virtualisation

In 5G practical deployments, the number of transmitter antenna elements at the gNB can be very large, often in the hundreds, to enable narrow beamforming and high spatial resolution, as discussed in Section 2.3.3. However, due to both standardisation constraints set by 3GPP and implementation limitations such as hardware costs, feedback overhead, and CSI reporting complexity [35], the number of CSI-RS ports that can be used for precoding and channel estimation is significantly lower. This is typically 4, 8, 12, or 16 ports, depending on the row number specified in TS 38.211 [8, Sec. 7.4.1.5], for which 4 and 8 CSI-RS ports are row numbers 4 and 6, respectively, whilst a massive MIMO array might contain 256 or 512 antenna elements. This means that each antenna element does not have its own CSI-RS port for transmitting reference signals and providing channel state feedback.

Subarray virtualisation addresses this by conceptually mapping groups of physical antenna elements to a smaller number of CSI-RS ports. The full antenna array is divided into multiple subarrays, each of which is associated with a CSI-RS port. The signals transmitted on each port are distributed across the subarray using predefined analogue or digital weightings. These are beamsteering vectors which are computed using MATLAB's `steervec` function within the Phased Array System Toolbox [33]. These vectors are averaged across elements in the subarray and normalised to form components of a virtual precoder, which is then applied at the transmission step, allowing the mapping of CSI-RS ports to the full antenna array. Due to MATLAB's validation checks between the number of antenna elements and CSI-RS ports, it is also necessary to virtualise the channel matrix estimate, $\mathbf{H}$, making sure that the dimensions are correct.

3.5 Performance Metrics

3.5.1 PDSCH Throughput and Spectral Efficiency

PDSCH throughput is evaluated by measuring the number of successfully decoded transport block bits over the total simulation time, normalised to Mbps, and as a percentage of the theoretical maximum as shown in Equation 3.1.

$$\text{Throughput (\%)} = \frac{\text{Total successful bits}}{\text{Total transmitted bits}} \times 100 \tag{3.1}$$

The throughput calculation is dynamically updated through HARQ retransmissions and CSI feedback. The theoretical maximum is derived from the transport block size, assuming

error-free transmission, allowing a baseline to quantify performance in non-ideal conditions such as channel estimation, imperfect CSI, and actual PDSCH channel performance across varying SNR.

Some academic papers may use spectral efficiency instead of throughput for their metric of performance. Spectral efficiency is, however, proportional to throughput and can be evaluated by measuring the number of successfully decoded transport block bits over the total simulation time and bandwidth. As our choice of bandwidth is constant at 40 MHz, the throughput is proportional to the spectral efficiency.

$$\eta = \frac{\text{Total bits successfully decoded}}{\text{Total time} \times \text{Bandwidth}} \tag{3.2}$$

3.5.2 Block Error Rate

Block Error Rate (BLER) is evaluated by measuring the number of transport blocks that are unsuccessfully decoded at the receiver over the total number of transmitted blocks, as shown in Equation 3.3.

$$\text{BLER} = \frac{\text{Number of transport blocks received in error}}{\text{Total number of transmitted blocks}} \tag{3.3}$$

In this simulation, a block error occurs if any codeword within a transport block fails a cyclic redundancy validation after decoding, including any HARQ retransmissions. According to 3GPP specification TS 38.214 [2, Sec 5.2.1.1], link adaptation mechanisms are designed to maintain a target BLER of 10%, to maintain throughput and robustness. A low BLER indicates high reliability and effective error correction, whereas a high BLER highlights the limits of channel estimation, CSI accuracy, and choice of coding schemes. By examining BLER alongside throughput over a range of SNRs, the trade-off between reliability and spectral efficiency can be assessed.

3.6 Parallel Computing

Due to the computation intensity of simulating an end-to-end 5G NR system over a wide range of SNR values and channel conditions, parallel computing techniques were employed to accelerate the simulation process. MATLAB's Parallel Computing Toolbox [36] was used in conjunction with `parfor` loops to parallelise the simulation. Since throughput and BLER measurements at each SNR point are independent, they are well-suited for parallel execution across multiple workers.

Simulations were executed on Amazon Web Services (AWS) EC2 on-demand platforms using the `r6i.8xlarge` instance type. This instance provides 32 vCPUs and 256 GB of RAM. This allows for the deployment of 31 workers for each of the 31 SNR points, ranging from -5 dB to 25 dB, in parallel. This configuration significantly reduced simulation times.

Each SNR point simulation was configured with `NFrames = 50`, which, given the numerology and subcarrier spacing selected, corresponds to 1000 slots per SNR point. We perform a Monte Carlo averaging across all slots to ensure that each BLER and throughput measurement is statistically reliable.

4. Results and Discussion

4.1 Simulation Framework Validation

A simulation framework involving the processing chain in Figure 3.1 was implemented using MATLAB's 5G Toolbox with the use of the `nrCDLChannel` object to model CDLs. As each of the transmission features, such as CSI feedback, HARQ, and channel estimation, was implemented, a series of validation tests were conducted against benchmarking scenarios. This was done to evaluate the performance effect of each implementation and ensure that they were in line with the findings of the literature review. The configuration parameters used for the results are listed in Table 3.1, where the controlled variables for each of the validation tests are specified. Then, different CDL profiles, Doppler, and MIMO configurations were employed and analysed in comparison to related literature or industry reports. For our initial validation tests, we configured our simulation to be 8Tx/4Rx with AAV option three discussed in Section 2.6, 4-layer CDL-C, with a delay spread of 300 ns and a Doppler shift of 10 Hz.

4.1.1 CSI Feedback Implementation

CSI feedback, described in Section 2.3.4, was implemented based on SU-MIMO type 1 PMI codebooks with both PMI follow and random. Follow refers to the selection of a PMI precoding matrix based on the best performance given the CSI-RS at that time. In contrast, random refers to a randomly selected PMI without any CSI feedback. RI for link adaptation (layer) and CQI for MCS and target code rate adaptation were also implemented for fullness with fixed RI and fixed CQI performance. A throughput percentage against a range of SNR between -5 to 25 with increment 1 and 1000 slots each point is computed and plotted in Figure 4.1. We observe that PMI follow performs minimally better in throughput ($\approx$ 0.2dB) than PMI random. This is expected, as the implementation of PMI random was not entirely random and depended on setting a random seed for PMI follow.

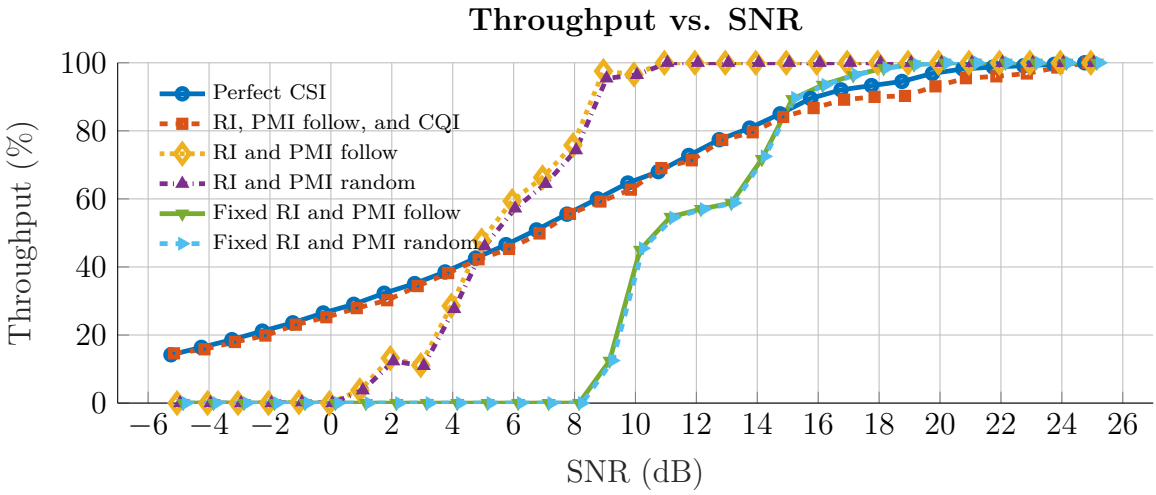

Figure 4.1: Throughput against SNR for CSI feedback implementation

For the perfect CSI and the RI, PMI follow, and the CQI configuration has a smooth throughput curve across all SNRs, with the ideal CSI outputting higher throughput

throughout. The perfect CSI assumes that the gNB has complete knowledge of the instantaneous channel with optimal precoding, meaning that there is no feedback overhead or quantisation as opposed to the CSI feedback implementation. This computes the maximum achievable throughput for any given end-to-end system.

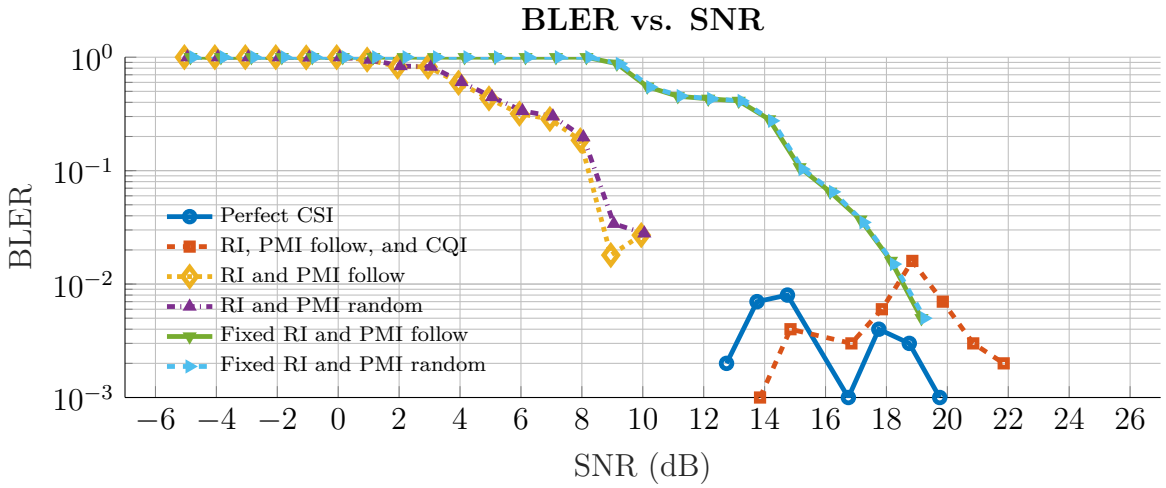

Figure 4.2: BLER against SNR for CSI feedback implementation

A fixed MCS of index 13 from the 64QAM table [2, Sec. 5.1.3.1] is applied, where the table derives the target code rate based on achieving below 10% BLER. We observe that the throughput at low SNR regions is zero for the fixed CQI curve. This is due to an aggressive MCS being used, which achieves high spectral efficiency but is fragile to noise. Consequently, the UE cannot reliably decode the transport block, resulting in zero throughput.

In Figure 4.2, BLER against SNR is plotted, and we observe that for a fixed MCS, BLER = 1 when the throughput is zero. For a fixed MCS, we can also see that when the BLER intersects the 10% line, this is where it roughly intersects with the adaptive MCS curve. This is due to adaptive MCS being selected to achieve BLER less than 10%, as shown, where no data point suggests 0% BLER. It is interesting to note that the throughput in mid-high SNR regions for a fixed MCS case is much higher than that of the perfect CSI case. This is unexpected, as we expect the perfect CSI to compute the maximum achievable throughput. A reason why this might be the case is due to how adaptive MCS is selected based on the threshold BLER; the selected MCS may be too aggressive for mid-SNR regions. Overall, this results in a -3 dB and 4dB SNR gain at 30% and 70% throughput, respectively.

A fixed RI, e.g. fixed layer, is implemented using a rank restriction at layer 4. As discussed in Section 2.3.1, the channel capacity is dependent on the number of parallel data streams, i.e. layers available, and the SNR. This means that for low SNR regions, one layer performs best, whilst for high SNR regions, four or more layers perform. We observe this when comparing RI and fixed RI throughput curves. We can see that the RI of all four layers performs better at both low and high SNRs as opposed to just layer 4, where throughput is only visible at high SNRs. This maintains a performance gain of $\approx$5 dB throughout. This confirms that our CSI feedback implementation aligns with the literature review, and we proceed with implementing HARQ retransmissions. We should also note that fixing RI induces this "dipping" effect due to layer mismatching and spatial

interference dominating at certain SNRs.

4.1.2 No HARQ vs. HARQ

To isolate the performance impact of implementing HARQ, we choose to have a fixed RI at layer 4, random PMI selection, and a fixed MCS of index 13 in the 64QAM table, and this is the case for the rest of the result cases unless specified. In earlier sections, HARQ was explained to retransmit failed transport blocks and combine them at the receiver, in turn reducing BLER and increasing overall throughput. Alsharbaty et al. [31] conclude from their study of HARQ that retransmissions cause temporary reductions in throughput.

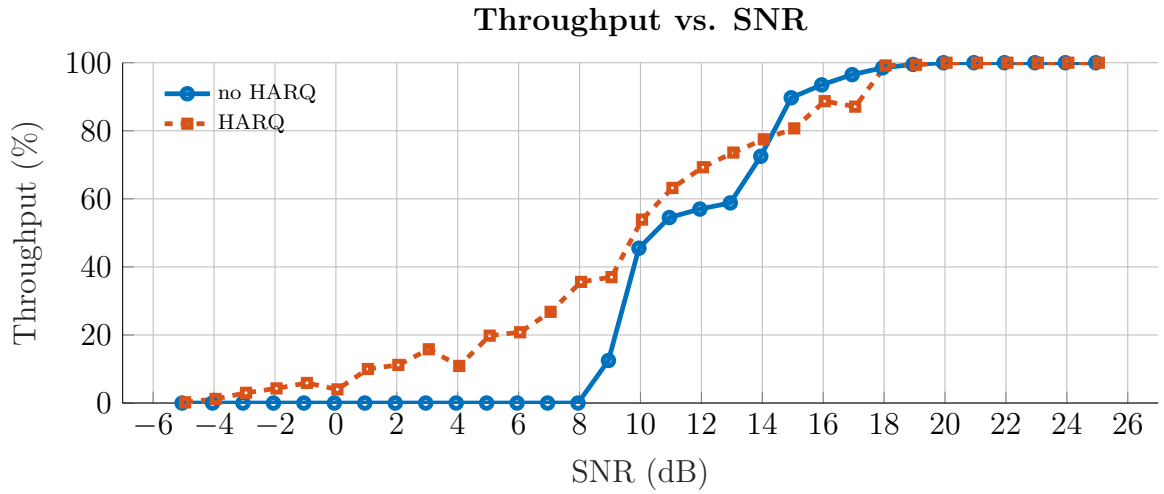

Figure 4.3: Throughput against SNR for HARQ implementation

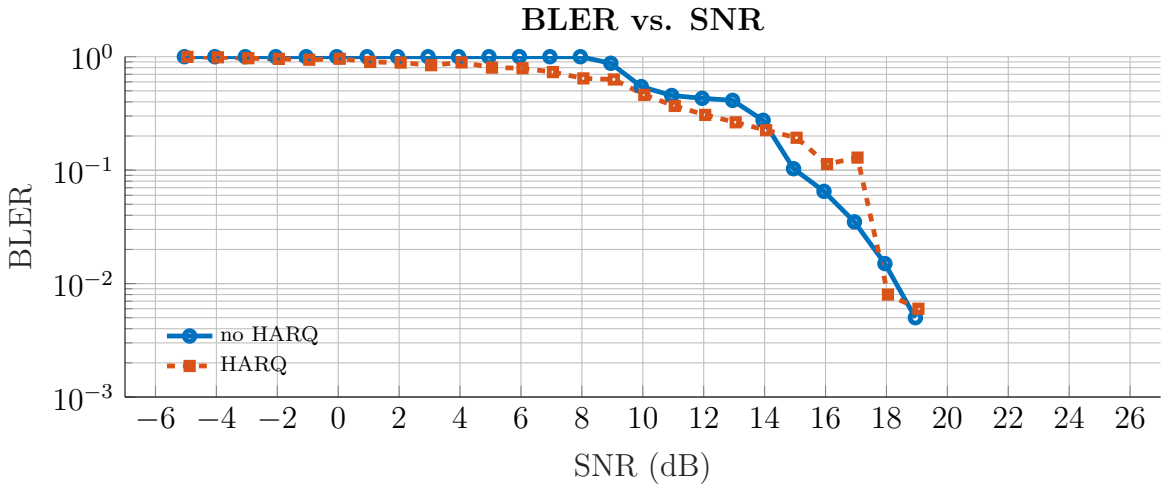

Figure 4.4: Throughput against SNR for HARQ implementation

Figure 4.3 and 4.4 show the plots of throughput percentage and BLER against SNR, respectively. We observe, however, for the 4-layer, this "dip" effect is more apparent in the no HARQ configuration. This is because the temporary reductions are more apparent in higher ranks, as observed in the industry data in Section 2.6, and these "dips" are in fact caused by the poor layer matching and thus, spatial interference. If we look at the BLER curve, the effect of retransmission is more apparent, where BLER is higher but then improves significantly after a successful transmission around 16-20 dB. Overall, with

HARQ at 30% and 70% throughput, there is a performance gain of 2 dB and 1.5 dB, respectively.

4.1.3 Ideal vs. Non. Ideal Channel Estimation

As HARQ for the 4-layer has improved the stability of the curve, which helps isolate throughput effects of further tests, HARQ was implemented unless specified. In Section 2.3.5, channel estimation through DM-RS is discussed to estimate the channel matrix based on known pilot symbols. Perfect channel estimation is where the receiver is assumed to have full knowledge of the true channel matrix.

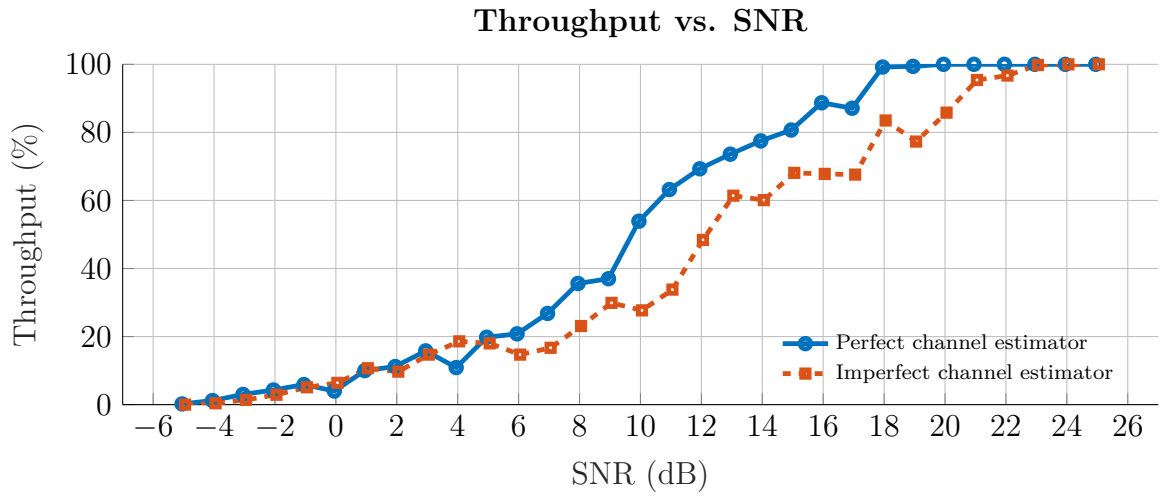

Figure 4.5: Throughput against SNR for channel estimation implementation

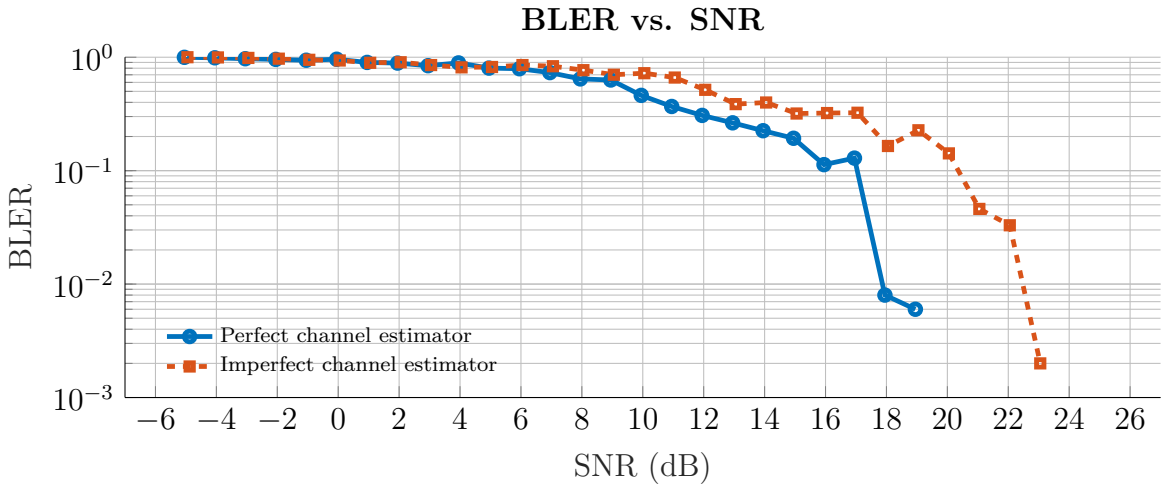

Figure 4.6: BLER against SNR for channel estimation implementation

We implement a DM-RS based channel estimation using least squares and compute the throughput and BLER against SNR in Figures 4.5 and 4.6, respectively. As a least squares estimator only directly solves for the minimal squared error, it is invariant to noise and hence a poor estimate, so the performance difference compared to the perfect case is not large ($\approx$ 2 dB loss). However, in low SNR conditions, we observe that for the perfect and imperfect channel estimators, the throughput and BLER are very similar. This is because in low SNR conditions, AWGN noise dominates over channel conditions, which the receiver cannot account for, resulting in high transport block errors (≈ 1) as shown.

4.1.4 Feature Degradation Under Realistic Assumptions

Now that we have implemented all of the features in a 3GPP standard 5G NR downlink system, the throughput and BLER against SNR curves between an ideal case (PMI follow, link adaptation, perfect channel estimator, no HARQ) and a realistic case (PMI random, fixed RI, least sqaures channel estimator, HARQ) is compared in Figures 4.7 and 4.8, respectively. MCS is fixed to observe the BLER improvement over the range of SNRs. We observe that there is a performance loss of 5 dB and 8 dB at 30% and 70% throughput, respectively. As discussed before, the use of a better channel estimator with noise covariance, such as MMSE, could potentially increase the performance loss, especially at mid-high SNR regions.

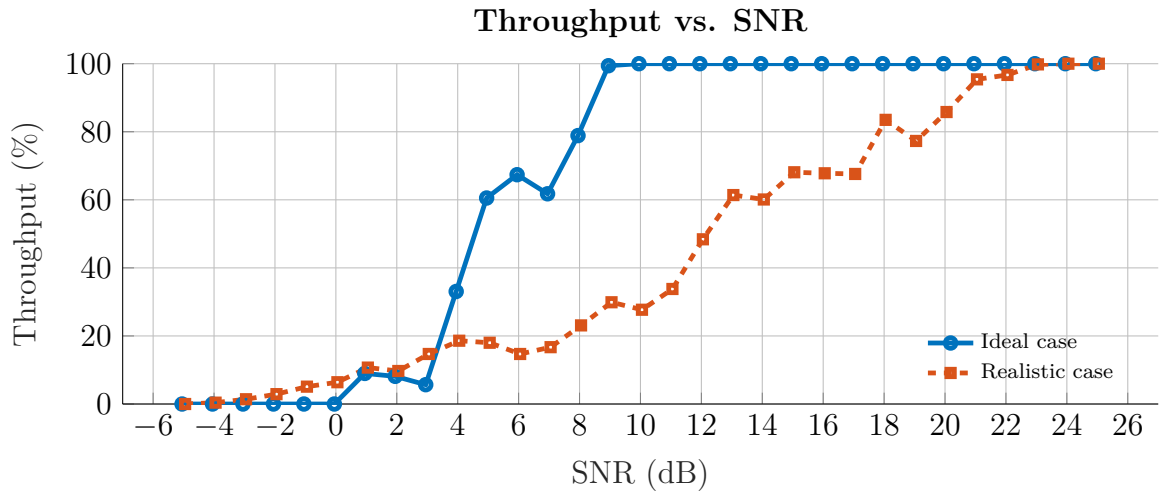

Figure 4.7: Throughput against SNR for ideal and realistic cases

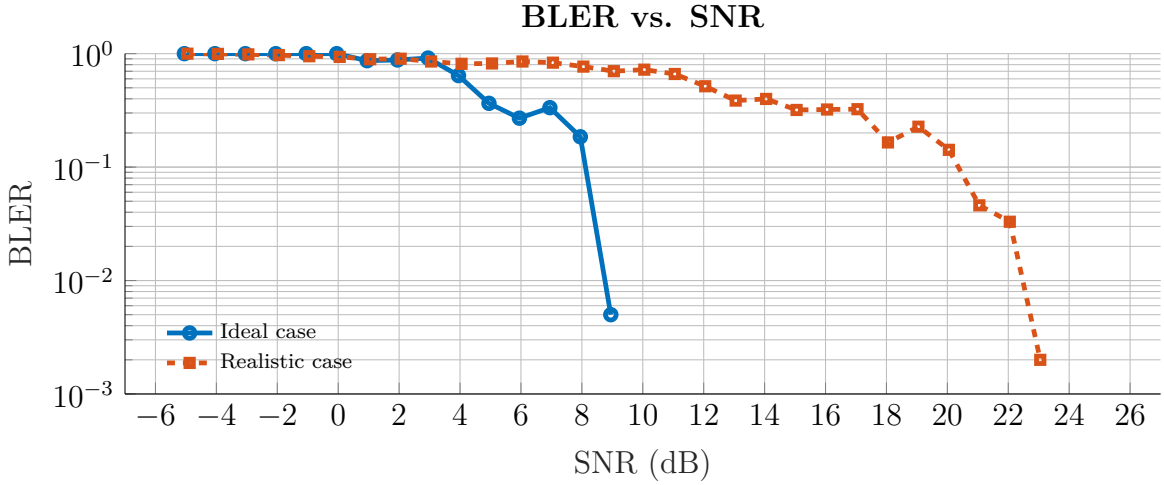

Figure 4.8: BLER against SNR for ideal and realistic cases

4.2 CDL Model Profiles

As a realistic case, it has been simulated and verified, in accordance with 3GPP specifications, literature, and industry reports, different 38.901 CDL models are evaluated to

accurately depict their use cases within a practical setting. Pessoa et al. [20] discuss how CDL-A models offer higher potential throughput due to multiple strong eigenmodes; variability in the channel could lead to inconsistent performance, especially in scenarios with rapid channel fluctuations. Pessoa et al. also describe that CDL-D provides more consistent throughput, but the dominance of a single eigenmode may limit the maximum achievable throughput in higher-order MIMO systems. Baghous [22], on the other hand, compares the performance between CDL-C/A/B models and concludes that the highest throughput was achieved in that descending order.

The different 38.901 CDL models are used, and the throughput against SNR is plotted in Figure 4.9 with a constant delay spread of 300 ns.

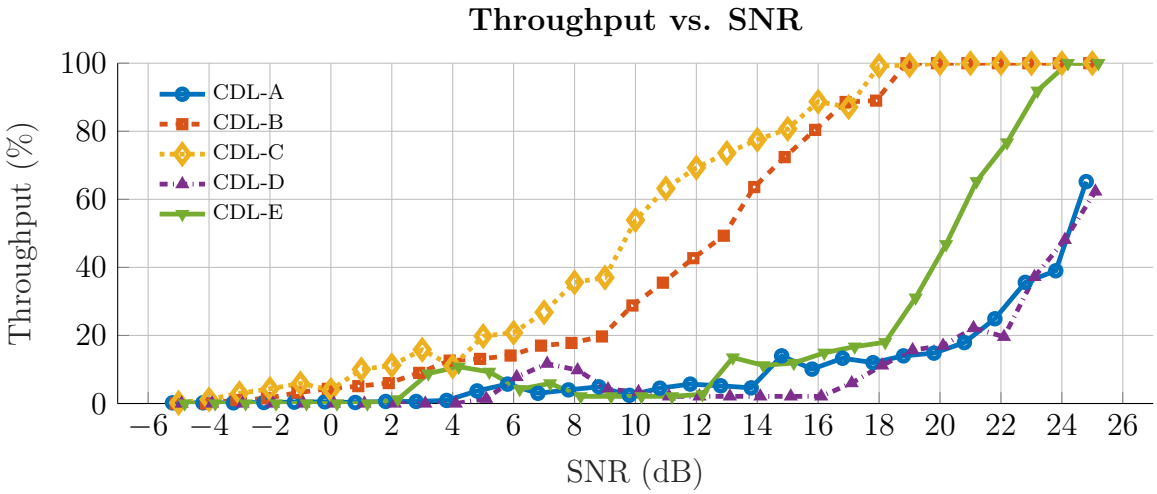

Figure 4.9: Throughput against SNR for different 38.901 CDL model profiles

We observe that the CDL-C model performs the best due to rich angular spread and strong multipath components, followed by CDL-B. This is contrary to what Baghous [22] found, and this is due to how the angular spreads for the CDL-A and the CDL-B are configured. In Table 2.1, we discussed that for the CDL-A model, low-scattering short-range links are its best use case due to wide angular spreads. However, for our configuration, we place our gNB and UE 100m away from each other, requiring narrow angular spreads. This is the reason why the CDL-B, which has a narrow angular spread, performs much better than the CDL-A. As with the CDL-A model, since the CDL-D model also has this property, it does not perform very well in our setup. For the CDL-E model, as the model is strongly LOS-dominated, there is likely only a single eigenmode dominant, limiting maximum achievable throughput at lower SNRs due to higher channel rank, as Pessoa et al. [20] discussed.

4.3 Doppler Shift

For an FR1 carrier frequency of 3.5 GHz, 10 and 100 Hz Doppler shifts correspond to 3 and 30 km/h UE speeds, respectively. This models the speeds of pedestrian movement and slow urban driving or cycling. We model these scenarios and compute the throughput and BLER against SNR to observe the effect of increasing Doppler in Figure 4.10. We observe that increasing the Doppler from 10 Hz to 100 Hz decreases our performance by around 2 dB and 5 dB at 30% and 70% throughput, respectively.

This is expected as Pawase and Chang [29] suggest that significant Doppler shifts lead to rapid channel variations. Our least squares estimate cannot keep up with the high mobility conditions and hence leads to a larger number of decoding errors. In industry reports shown in Figure 2.8 for an 8Tx/4Tx 4-layer configuration for CDL option 2 (untruncated), the performance loss between 10 Hz and 100 Hz Doppler was ≈ 0.5 dB, as opposed to our performance loss of 2-5 dB. We may assume that each vendor has adapted their channel estimation schemes, likely with temporal considerations as Kim et al. [30] highlights the importance of, which involve minimal dB loss in high mobility cases.

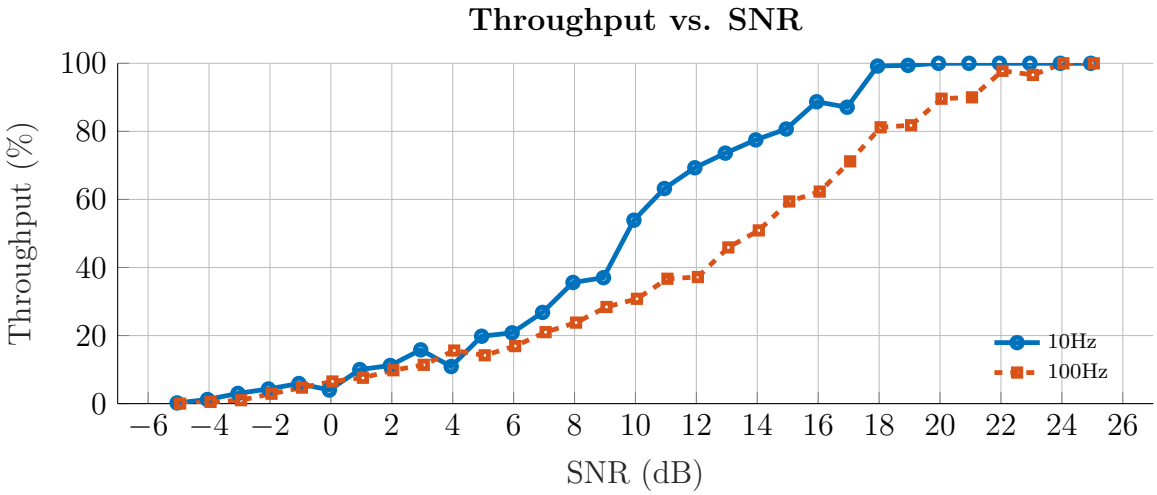

Figure 4.10: Throughput against SNR for different Doppler cases

4.4 MIMO Layer and Industry Comparison

The variation in MIMO configuration and the number of layers, aligned with the industry reports for option three discussed in Section 2.6, was evaluated and plotted in Figure 4.11. We first observe that between the control case of 8Tx/4Rx 4-layer against 4Tx/4Rx 4-layer, there is a performance gap of around 4-5 dB in the mid SNR regions. This is expected and in line with Baghous' findings [22] that the increase in the number of Tx elements results in higher throughput due to a higher bit contribution to the receiver. Although the channel rank is limited by the minimum of the number of Tx and Rx elements, the quality of the channel matrix improves with Tx as more spatial directions are available, allowing a better channel estimate.

As we increase the number of MIMO layers, the capacity of the channel increases along with SNR as discussed in Section 2.3.1. This means that for lower ranks, hence lower layers, the capacity of the channel is reached at lower SNRs than for higher ranks, as shown in the max throughput values in Table 4.1. This is observed between the 2-layer and 8-layer cases. An exception to this is the 4Tx/4Rx 4-layer case, where it underperforms considerably compared to the other cases. This is because although the max channel rank is four, the actual channel rank is around two, which is common in many practical CDL scenarios as discussed by Pessoa [20]. For the 8-layer case, on the other hand, makes use of two separate codewords with each rank = 4, which resolves this issue. Codeword 1 denotes the mapping to the first four layers, whereas codeword 2 denotes the mapping to the second four layers. As the first 4-layers reach capacity at lower SNR regions than

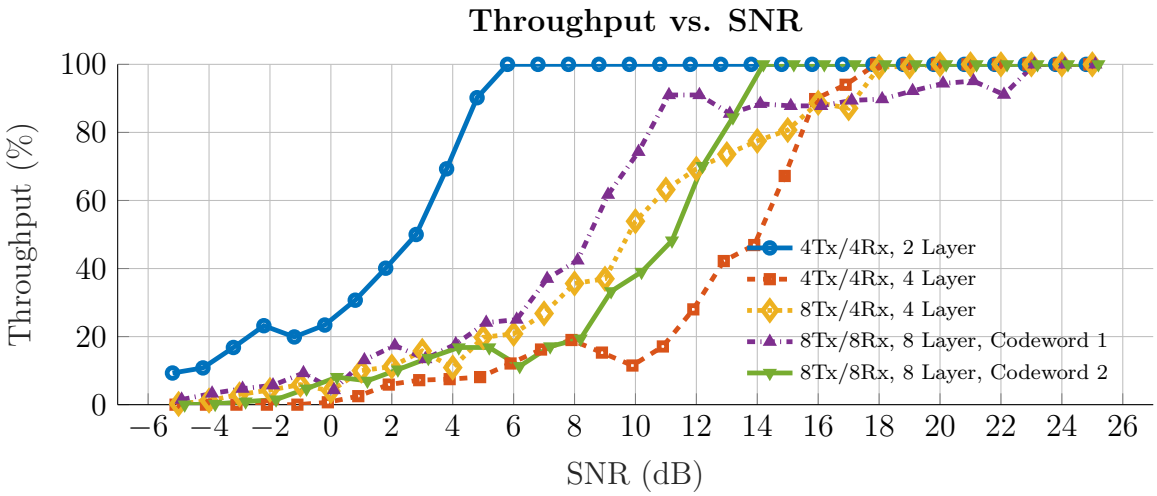

Figure 4.11: Throughput against SNR for different MIMO layers and configurations

the latter layers, this explains the difference in performance and max capacity of the two codewords. We also note that there is a plateau for codeword one before reaching capacity. This may be due to the HARQ retransmission "dipping" effects discussed earlier, which are more evident for higher layers, also seen in industry simulations.

Number of MIMO layers	Max Throughput (bits)	SNR (dB) at Throughput	
		30%	70%
2	38936000	0.5	4
4 (4Tx)	77896000	12	15
4 (8Tx)	73776000	7	12
8 (Codeword 1)	43032000	6.5	9.5
8 (Codeword 2)	58384000	9	12

Table 4.1: Max throughput and SNR thresholds at 30% and 70% throughput for varying MIMO layers.

In Table 4.1, the SNRs at throughput 30% and 70% are shown for each MIMO configuration. For the 4Tx/4Rx 4-layer case, 12 dB and 15 dB were achieved, and in the industry simulations for AAV option 3, CDL option 2 in Table 2.3, 6.8 dB and 15.7 dB were achieved on average with a span of 2.7 dB and 1.7 dB, respectively. This data is plotted in Figure 4.12 in comparison to our simulations. Although for the 70% throughput, our simulation results were concordant with industry data, for 30% our results differed by 5.2 dB. One potential factor contributing to the discrepancy between simulation and industry-report low-SNR performance is the use of ray splitting in CDL stated in 3GPP RAN4 Topic Summary for NR_SCM[32, Issue 4-1-6]. Ray splitting divides each multipath component into sub-rays with slight angular and delay offsets, enhancing angular diversity and increasing channel rank. This tackles the problem of actual channel rank discussed by Pessoa [20]. Consequently, our channel is limited at an actual lower rank, resulting in the underestimation of performance, particularly at lower SNRs, as observed in Figure 4.12.

In Tables 2.4 and 2.5 show that the average achieved SNRs between vendors at 30% and 70% throughput for codewords 1 and 2 was 6.5 dB, 17.4 dB and 12.5 dB, 26.8 dB with

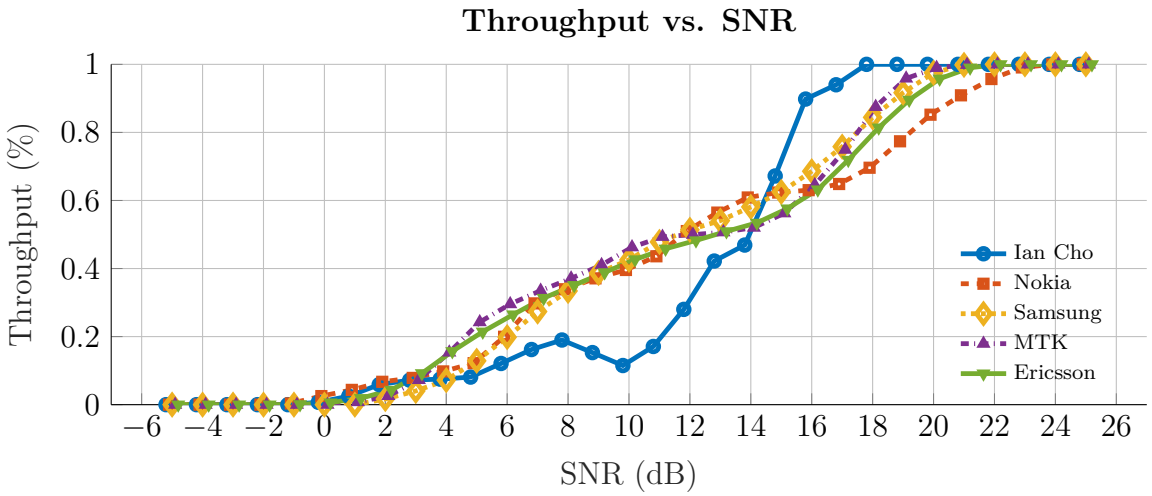

Figure 4.12: Throughput against SNR alignment for AAV option 3, 4-layers

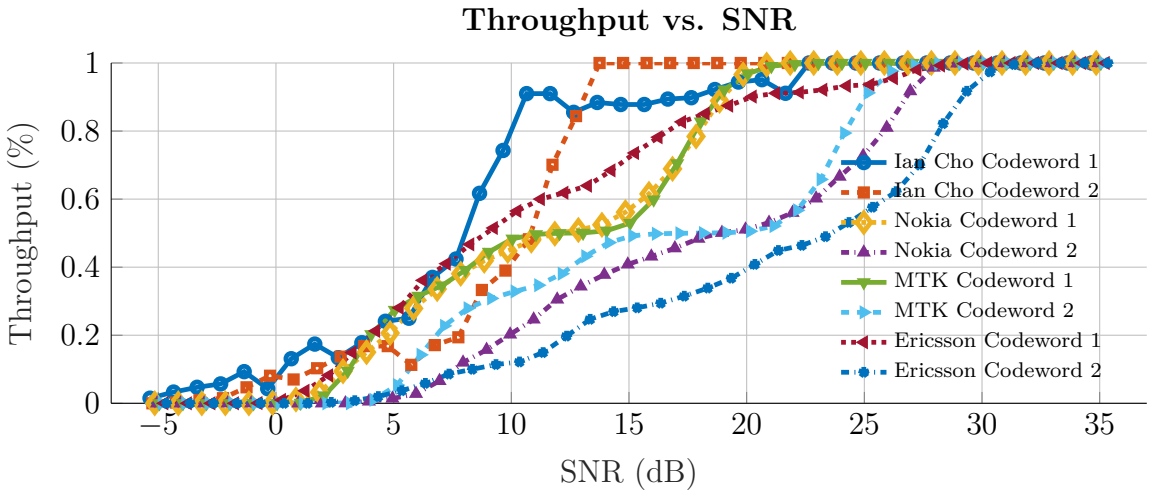

Figure 4.13: Throughput against SNR alignment for AAV option 3, 8-layers

a span of 5.9 dB, 7.2 dB and 5.8 dB, 11.3 dB, respectively. Our simulations achieved SNRs 6.5 dB, 9.5 dB and 9 dB, 12 dB at 30% and 70% throughput for codewords 1 and 2, respectively. Figure 4.13 shows the comparison between vendors and our simulation. For our 30% throughput SNR values, they are inline with the industry-reported data, but at 70% throughput, we observe a large disparity in SNR, with the simulations achieving much higher performance. This is attributed to our implementation of channel estimation. As least squares estimation is used and it is not variant to noise, least squares may often overestimate throughput due to overconfident CSI, particularly in mid-high SNR regions, which is shown in both Figures 4.13 and 4.12. However, it is noted that data between vendors is inconsistent, but we observe that our data is most aligned with Nokia and MTK at low SNR ranges.

4.5 Subarray virtualisation of Massive MIMO

Subarray virtualisation of massive MIMO transmitter antenna was implemented in agreement with option 1Y 4-layer of the 3GPP industry reports. Option 1Y has an AAV configuration of [8 4 2 8 1] corresponding to 512 Tx elements for 8 CSI-RS ports, and

Option 3 has an AAV configuration of [1 4 2 1 1] corresponding to 8 Tx elements. As discussed, Baghous [22] concludes that enabling massive MIMO antenna arrays should increase overall throughput due to larger arrays allowing sharper and narrower beamforming and more spatial degrees of freedom. In Figure 4.14, we observe that at 30% and 70% throughput, there is a performance loss of 11 dB and 7 dB, respectively. However, when compared to industry data in Figure 4.15, there is a performance difference of 4.5 dB and -1.5 dB for 30% and 70% throughput, respectively. Again, for the same reasons discussed in the previous section, we achieve lower performance at 30% throughput due to not implementing ray splitting and higher performance at 70% throughput due to different channel estimation techniques.

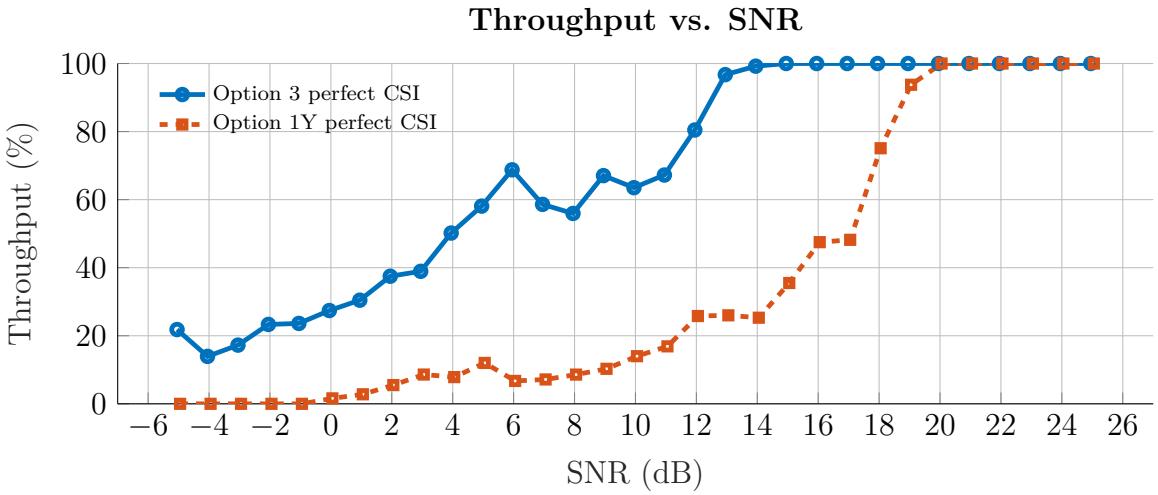

Figure 4.14: Throughput against SNR for subarray virtualisation implementation at 8Tx/4Rx 4-layer

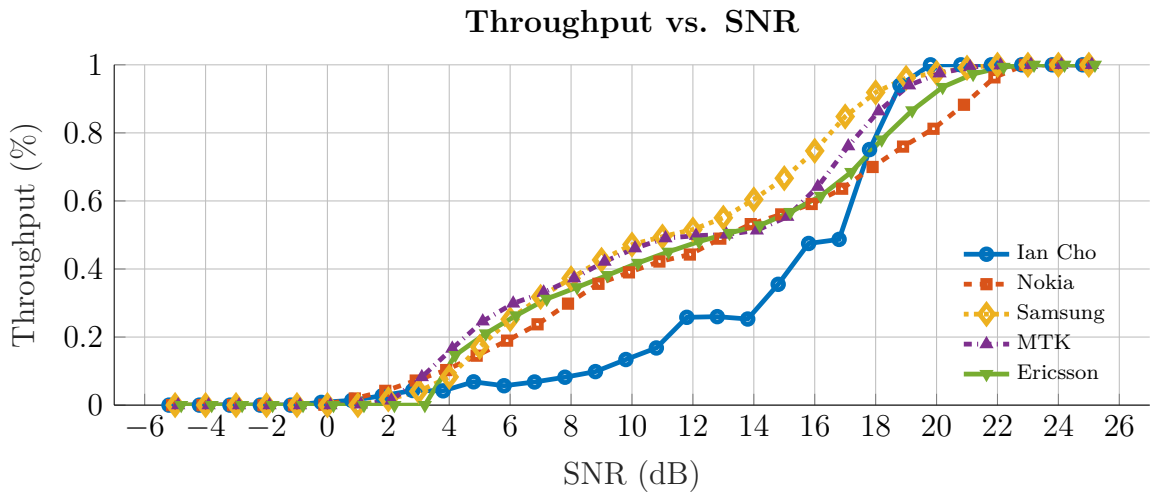

Figure 4.15: Throughput against SNR alignment for AAV option 1Y, 4-layers

5. Conclusion

5.1 Summary of Project Objectives and Approach

This project set out to investigate the extent to which CDL-defined channel environments influence the practical gains of MIMO techniques in an end-to-end downlink 5G NR system. To achieve this, a series of technical objectives was defined to guide the implementation and methodology. First, a controlled but flexible simulation framework to model an end-to-end PDSCH 5G NR system is constructed to evaluate throughput and BLER. Transmission features such as HARQ, CSI feedback, and channel estimation are implemented systematically and performance is compared with existing studies and industry reports to ensure validity of design. Second, the performance of different CDL profiles is evaluated to characterise each of their use cases. Lastly, different MIMO configurations and Doppler shifts are explored, and the extent to which CDL-defined channel environments influence the practical gains in typical deployment scenarios is assessed.

5.2 Contributions

The following list summarises the main technical contributions achieved during the development and evaluation phases of this project:

- Systematically developed a 3GPP-compliant MATLAB simulation framework capable of evaluating PDSCH throughput and BLER. Implemented support for realistic feedback mechanisms, including codebook-based CSI reporting (RI, PMI, CQI) and their impact on throughput. The limitations of perfect CSI and channel estimation were explored, demonstrating that idealised feedback models may overestimate performance compared to realistic feedback.
- Performed comparative analysis between different 3GPP-defined TR 38.901 CDL models. Throughput degrades in spatially rich CDL scenarios (i.e. rich urban compared with rural areas), and CDL profiles with narrower angular spreads perform well when the base station is directed straight towards the UE.
- Investigated the disparity in performance under different mobility scenarios. Throughput degrades with higher UE speeds such as pedestrian walking compared to slow urban driving or cycling. The performance loss is dependent on the quality of the channel estimation, especially if temporal effects are considered.
- Investigated the influence of MIMO layers and antenna configuration. Performance gain from the addition of MIMO layers is strongly dependent on accurate CSI and channel modelling. Inaccurate and non-ideal CSI suffers from saturation of the maximum channel rank.
- Integrated subarray virtualisation to allow massive MIMO antenna arrays to be mapped to a limited number of CSI-RS ports, emulating real-world gNB constraints. Given the same number of layers, for ideal CSI and channel estimation, the performance decreases by 7 dB to 11 dB throughout.
- Benchmarked simulation results against vendor submissions to 3GPP RAN4 meetings. Comparisons with vendor-reported results show similar throughput trends between different MIMO layers, but results diverge due to simplified channel estimation and saturation of channel rank without the implementation of 38.753 CDL-defined features such as ray splitting.

5.3 Limitations and Implications for Real Systems

This project, whilst aligned with 3GPP standards, has certain limitations that affect the direct applicability of its results to real-world systems:

- Idealised assumptions: Hardware impairments, RF non-linearities, and protocol stack latencies were not modelled. As a result, the performance metrics may be optimistic compared to practical deployments.
- Partial CSI feedback: Quantisation, predictive lag and delay were simplified. Link adaptation and adaptive MCS selection using RI and CQI, respectively, were fixed for controlled benchmarking. This significantly impacts the precoding accuracy and system capacity in practical deployments
- Simplified channel estimations: Vendor-specific estimation techniques like MMSE, ZF and Kalman filtering were not implemented, and instead a least squares estimator was used. Hence, channel noise and temporal effects were not considered, and performance was overestimated, particularly at high SNR regions.
- Subarray virtualisation constraints: Only perfect channel assumptions and analogue beamsteering were modelled, and larger antenna arrays were not investigated. In practice, a hybrid of analogue and digital beamsteering techniques is used with a variety of large antenna array sizes depending on the deployment scenario.
- Computation constraints: Only `Nframes = 50`, which corresponds to 1000 slots per SNR point, was used with Monte Carlo convergence. The 95% confidence interval for throughput estimates is expected to lie within $\pm$0.3-0.6% of the mean.

Despite these limitations, the findings remain highly relevant to real-world system design. The observed trends, such as performance degradation under imperfect CSI, Doppler effects, and between MIMO layers, directly reflect the challenges faced in deploying high-capacity 5G networks. When compared to industry data, although there was a divergence, especially at the mid-SNR ranges, which was attributed to channel estimation simplifications and model differences between the 38.901 and 38.753 CDL, there was alignment in demonstrating trends between different MIMO configurations and feature effects, such as HARQ. Therefore, this project makes a meaningful contribution to ongoing discussions on benchmarking and channel model refinement for Release 19 and beyond.

5.4 Future Work

Whilst this project has established a robust framework for evaluating 5G NR downlink performance under standardised CDL models, several extensions remain open for exploration. One direction for future work is the integration of advanced channel estimation techniques, such as Kalman filtering or machine learning-based predictors, to account for Doppler effects. Additionally, further work could expand support for multi-user MIMO scenarios to reflect more complex scheduling environments or the implementation of hybrid beamsteering to provide insights into realistic massive MIMO deployment scenarios. Lastly, as Release 19 and TR 38.753 continue to evolve, modelling a custom CDL profile with features like ray splitting and comparing against future industry submissions would offer ongoing relevance and contribute meaningfully to the development of standardisation benchmarks.

Bibliography

[1] E. Dahlman, S. Parkvall, and J. Skold, *5G NR: The Next Generation Wireless Access Technology*, 1st. Academic Press, 2018, ISBN: 978-0-12-814324-7. [Online]. Available: https://learning.oreilly.com/library/view/5g-nr-the/9780128143247/.

[2] "NR; Physical layer procedures for data," 3rd Generation Partnership Project (3GPP), Tech. Rep. 3GPP TS 38.214 V18.6.0, Mar. 2025. [Online]. Available: https://www.etsi.org/deliver/etsi_ts/138200_138299/138214/18.06.00_60/ts_138214v180600p.pdf.

[3] "Study on channel model for frequencies from 0.5 to 100 ghz," 3rd Generation Partnership Project (3GPP), Technical Report 3GPP TR 38.901 V18.0.0, May 2024. [Online]. Available: https://www.etsi.org/deliver/etsi_tr/138900_138999/138901/18.00.00_60/tr_138901v180000p.pdf.

[4] D. G. Riviello, F. Di Stasio, and R. Tuninato, "Performance analysis of multi-user mimo schemes under realistic 3gpp 3-d channel model for 5g mmwave cellular networks," *Electronics*, vol. 11, no. 3, p. 330, 2022, ISSN: 2079-9292. DOI: 10.3390/electronics11030330.

[5] G.-R. Barb, M. Otesteanu, G. Budura, and C. Balint, "Performance evaluation of tdl channels for downlink 5g mimo systems," *2019 International Symposium on Signals, Circuits and Systems (ISSCS)*, pp. 1–4, 2019. DOI: 10.1109/ISSCS.2019.8801790.

[6] ETSI MCC, "RAN4#115 Meeting Report," 3GPP RAN4, Tech. Rep. R4-2505300, 2025. [Online]. Available: https://www.3gpp.org/ftp/tsg_ran/WG4_Radio/TSGR4_115/Docs/R4-2505300.zip.

[7] MathWorks, *5g toolbox documentation*, Accessed: January 21, 2025, n.d. [Online]. Available: https://uk.mathworks.com/help/5g/.

[8] "NR; Physical channels and modulation," 3rd Generation Partnership Project (3GPP), Tech. Rep. 3GPP TS 38.211 V18.6.0, Mar. 2025. [Online]. Available: https://www.etsi.org/deliver/etsi_ts/138200_138299/138211/18.06.00_60/ts_138211v180600p.pdf.

[9] "NR; Multiplexing and channel coding," 3rd Generation Partnership Project (3GPP), Tech. Rep. 3GPP TS 38.212 V18.6.0, Mar. 2025. [Online]. Available: https://www.etsi.org/deliver/etsi_ts/138200_138299/138212/18.06.00_60/ts_138212v180600p.pdf.

[10] "NR; Base Station (BS) radio transmission and reception," 3rd Generation Partnership Project (3GPP), Tech. Rep. 3GPP TS 38.104 V18.9.0, Mar. 2025. [Online]. Available: https://www.etsi.org/deliver/etsi_tr/138900_138999/138901/18.00.00_60/tr_138901v180000p.pdf.

[11] "Evolved Universal Terrestrial Radio Access (E-UTRA); Physical Channels and Modulation (Release 17)," 3rd Generation Partnership Project (3GPP), Tech. Rep. 3GPP TS 36.211 V18.0.1, 2024. [Online]. Available: https://www.etsi.org/deliver/etsi_ts/136200_136299/136211/18.00.01_60/ts_136211v180001p.pdf.

[12] "NR; NR and NG-RAN Overall Description," 3rd Generation Partnership Project (3GPP), Tech. Rep. 3GPP TS 38.300 V18.5.0, 2025. [Online]. Available: https://www.etsi.org/deliver/etsi_ts/138300_138399/138300/18.05.00_60/ts_138300v180500p.pdf.

[13] L. Vangelista and M. Centenaro, "Performance evaluation of harq schemes for the internet of things," *Computers*, vol. 7, no. 4, p. 48, 2018, ISSN: 2073-431X. DOI: 10.3390/computers7040048.

[14] ShareTechnote, *A comprehensive resource for wireless communication technologies*, Accessed: January 21, 2025. [Online]. Available: https://sharetechnote.com/.

[15] "Study on New Radio (NR) access technology: MIMO aspects," 3rd Generation Partnership Project (3GPP), Tech. Rep. 3GPP TS 38.912 V18.0.0, 2024. [Online]. Available: https://www.etsi.org/deliver/etsi_tr/138900_138999/138912/18.00.00_60/tr_138912v180000p.pdf.

[16] D. Tse and P. Viswanath, *Fundamentals of Wireless Communication*. Cambridge University Press, 2005.

[17] Samsung, "Massive mimo for new radio (nr) technical white paper," Samsung Electronics Co., Ltd., Tech. Rep., 2020. [Online]. Available: https://images.samsung.com/is/content/samsung/assets/global/business/networks/insights/white-papers/1208_massive-mimo-for-new-radio/MassiveMIMOforNRTechnicalWhitePaper-v1.2.0.pdf.

[18] Q. H. Spencer, A. L. Swindlehurst, and M. Haardt, "Zero-forcing methods for downlink spatial multiplexing in multi-user mimo channels," *IEEE Transactions on Signal Processing*, vol. 52, no. 2, pp. 461–471, 2004. DOI: 10.1109/TSP.2003.821107.

[19] M. Ferreira and F. H. Vieira, "Delay minimization based uplink resource allocation for device-to-device communications considering mmwave propagation," *PeerJ Computer Science*, vol. 7, e462, Apr. 2021. DOI: 10.7717/peerj-cs.462.

[20] A. M. Pessoa, L. M. de Carvalho, A. L. de Almeida, R. T. de Sousa, and J. A. Apolinario, "A CDL-based Channel Model with Dual-Polarized Antennas for 5G MIMO Systems in Rural Remote Areas," *ResearchGate Preprint*, 2020. [Online]. Available: https://www.researchgate.net/publication/344003028_A_CDL-based_Channel_Model_with_Dual-Polarized_Antennas_for_5G_MIMO_Systems_in_Rural_Remote_Areas.

[21] A. A. Mohamed, "The impact of numerology on the pdsch throughput of the 5g downlink," *Engineering, Technology & Applied Science Research*, vol. 14, no. 5, pp. 16 813–16 817, 2024. DOI: 10.48084/etasr.8370.

[22] J. Baghous, "5G System Throughput Performance Evaluation Using Massive-MIMO Technology with Cluster Delay Line Channel Model and Non-Line of Sight Scenarios," *Infocommunications Journal*, vol. 13, no. 2, pp. 24–29, 2021. [Online]. Available: https://www.infocommunications.hu/documents/169298/4713308/InfocomJ_2021_2_6_Baghous.pdf.

[23] M. A. T. Almahadeen and A. M. Matarneh, "Performance assessment of throughput in a 5g system," *Jordanian Journal of Computers and Information Technology (JJCIT)*, vol. 6, no. 3, pp. 303–316, Sep. 2020, ISSN: 2413-9351. DOI: 10.5455/jjcit.71-1590016486.

[24] ETSI MCC, "RAN4#114 Meeting Report," 3GPP RAN4, Tech. Rep. R4-2503100, 2025. [Online]. Available: https://www.3gpp.org/ftp/tsg_ran/WG4_Radio/TSGR4_114bis/Docs/R4-2503100.zip.

[25] 3rd Generation Partnership Project (3GPP), "Study on Performance Evaluation Methods for MIMO in NR," Tech. Rep. 3GPP TR 38.753, 2025, Draft, referenced in industry contributions, not publicly released at time of writing.

[26] BT, "TP for TR 38.753 Section 6.2 MU-MIMO," 3GPP RAN4, Tech. Rep. R4-2504616, 2025. [Online]. Available: https://www.3gpp.org/ftp/tsg_ran/WG4_Radio/TSGR4_114bis/Docs/R4-2504616.zip.

[27] BT, "Simulation Results for SCM Comparison and Alignment," 3GPP RAN4, Meeting Report R4-2502377, 2025. [Online]. Available: https://www.3gpp.org/ftp/tsg_ran/WG4_Radio/TSGR4_114/Docs/R4-2502377.zip.

[28] BT, "Results collection table for NR SCM," 3GPP RAN4, Tech. Rep. R4-2507823, 2025. [Online]. Available: https://www.3gpp.org/ftp/tsg_ran/WG4_Radio/TSGR4_115/Docs/R4-2507823.zip.

[29] C. J. Pawase and K. Chang, "5g-nr physical layer-based solutions to support high mobility in 6g non-terrestrial networks," *Drones*, 2023, ISSN: 2504-446X. DOI: 10.3390/drones7030176. [Online]. Available: https://www.mdpi.com/2504-446X/7/3/176.

[30] H. Kim, S. Kim, H. Lee, C. Jang, Y. Choi, and J. Choi, "Massive mimo channel prediction: Kalman filtering vs. machine learning," *CoRR*, 2020. [Online]. Available: https://arxiv.org/abs/2009.09967.

[31] F. S. A. Firas and S. H.Fasola, "The effect of harq procedure on the performance of lte system," *AL-Rafdain Engineering Journal (AREJ)*, vol. 22, pp. 123–122, Feb. 2014. DOI: 10.33899/rengj.2014.86989.

[32] Nokia, "Topic summary for [115][321] NR_SCM," 3GPP RAN4, Tech. Rep. R4-2507853, 2025. [Online]. Available: https://www.3gpp.org/ftp/tsg_ran/WG4_Radio/TSGR4_115/Docs/R4-2507853.zip.

[33] MathWorks, *Phased array system toolbox documentation*, Accessed: February 17, 2025, n.d. [Online]. Available: https://www.mathworks.com/help/phased/.

[34] W. Zhang, M. Li, and X. Chen, "Dynamically subarray-connected hybrid precoding scheme for mmwave massive mimo systems," *Wireless Communications and Mobile Computing*, pp. 1–12, 2021. DOI: 10.1155/2021/5528522.

[35] J.-C. Shen, J. Zhang, E. Alsusa, and K. B. Letaief, "Compressed csi acquisition in fdd massive mimo: How much training is needed?" *IEEE Transactions on Wireless Communications*, vol. 15, no. 6, pp. 4145–4156, 2016. DOI: 10.1109/TWC.2016.2535310.

[36] MathWorks, *Parallel computing toolbox documentation*, Accessed: March 05, 2025, n.d. [Online]. Available: https://www.mathworks.com/help/parallel-computing/.

A. Simulation Code, Logbook, Risk Assessment, and Ethical Statement

A.1 Simulation Code and Logbook

The simulation code used can be found in my GitHub repository: `https://github.com/ianwh02/NokiaIIBProject` under the folder '/Simulation/'. The logbook can be found in the file 'logbook.xlsx'.

A.2 Risk Assessment

A risk assessment to identify risks likely to be encountered during the project was carried out, and a form was submitted to the Safety Office at the start of the Michaelmas term. As this project is entirely carried out using a computer, there is minimal risk involved when working on the project. As the project progresses, High Performance Computing (HPC) may need to be accessed to simulate more computationally expensive simulations. Hence, this risk assessment was reflected accurately during the course of the project.

In retrospect, although there is minimal risk in the use of a computer, there is a slight risk of eye strain, especially during extended use. This should be added to one of the potential risks in the form.

A.3 Ethical Statement

This project involved MATLAB-based simulations of 5G NR physical layer performance and did not involve human participants, personal data, or environmental interaction. Ethical approval was therefore not required, and the research complies with the University of Cambridge's guidelines for responsible conduct of research.

B. Industry Simulation Results and Simulation Parameters

B.1 Summary of Industry Simulation Results

TDoc Number	Author	Title
R4-2502377	BT	Simulation Results for SCM Comparison and Alignment
R4-2503100	ETSI MCC	RAN4 #114 Meeting Report
R4-2503268	MediaTek Inc.	Downlink Simulation Results under CDL/TDL Models
R4-2503541	Apple	Downlink Throughput Simulation Results
R4-2503555	Nokia	Evaluation of PDSCH Performance in Multipath Fading
R4-2503659	Samsung	Simulation of 5G NR Throughput in CDL Scenarios
R4-2504003	ZTE Corportation, Sanechips	HARQ and MIMO Performance Evaluation
R4-2504181	Qualcomm	PDSCH Performance under CDL-E at High Mobility
R4-2504309	Huawei, HiSilicon	Comparative Study of TDL-A and CDL-C
R4-2504382	Ericsson	5G NR Link-Level Evaluation using CDL Models
R4-2505300	ETSI MCC	RAN4 #115 Meeting Report
R4-2505594	MediaTek Inc.	Simulation results of Spatial Channel Modelling
R4-2505902	Apple	Simulation results for Spatial Channel Modelling study
R4-2505957	Qualcomm	Simulation Results for SCM for demod
R4-2506173	Nokia	Discussion on Spatial Channel Model for Demodulation Performance Requirements
R4-2506677	Samsung	Simulation results on spatial channel model
R4-2506958	ZTE Corporation, Sanechips	Simulation results on spatial channel model for demodulation performance requirements
R4-2507045	Huawei, HiSilicon	Simulation results for SCM
R4-2507140	Ericsson	Simulation results for Rel-19 SCM for demodulation
R4-2507344	Huawei, HiSilicon	PMI simulation results for SCM
R4-2507823	BT	Results collection table for NR SCM
R4-2507824	BT	Simulation Results for SCM Comparison and Alignment
R4-2507853	Nokia	Topic summary for [115][321] NR_SCM

Table B.1: Table of 3GPP Tdocs containing industry simulation results, meeting reports, and topic summaries.

B.2 Industry Simulation Parameters

Parameter		Value
Duplex mode		TDD
TDD Slot Configuration Pattern		7D1S2U
FR / Carrier frequency		FR1, 3.5 GHz
UE Speed		3km/h
Antenna configuration		Rank 4: 4Tx, 4Rx Rank 8: 8Tx, 8Rx
Number of layers		8, 4
PMI		Random, Fixed
Waveform		CP-OFDM with normal CP
Channel Bandwidth/SCS		40 MHz / 30 kHz
MCS		13 (64 QAM table)
PDSCH configuration	Mapping type	Type A
	k0	0
	Starting symbol (S)	2
	Length (L)	12
	PDSCH aggregation factor	1
	Resource allocation type	Type 0
	VRB-to-PRB mapping type	Non-interleaved
	VRB-to-PRB mapping interleaver bundle size	N/A
PDSCH DMRS configuration	DMRS type	Type 1
	Number of additional DMRS	1
	Maximum number of OFDM symbols for DL front Loaded DMRS	Rank 4: 1 Rank 8: 2
Codebook configuration	Codebook type	Single Panel Type I
	Codebook configuration	4Tx: (N1, N2, O1, O2) = (2, 1, 4, 1) 8Tx: (N1, N2, O1, O2) = (4, 1, 4, 1)
PDSCH DMRS precoding configuration		Random: every PRB Bundle (size = 2) Fixed: Wideband PMI
NZP CSI-RS for CSI acquisition	CSI-RS resource type	Aperiodic
	Number of CSI-RS ports (X)	4 CSI-RS Ports (2, 1) for 4 Layer 8 CSI-RS Ports (4, 1) for 8 Layer
	Density (rho)	1
	First OFDM symbol in the PRB used for CSI-RS	(13)
Number of HARQ processes		8
Maximum HARQ transmissions		4
Channel models		CDL-UMa-C with (M, N, P, Ms, Ns) = (8, 4, 2, 8, 1) CDL-UMa-C with (M, N, P, Ms, Ns) = (8, 2, 2, 8, 1) CDL-UMa-C with (M, N, P, Ms, Ns) = (1, 4, 2, 1, 1) CDL-UMa-C with (M, N, P, Ms, Ns) = (1, 2, 2, 1, 1) TDL-C, XPL, medium
Test metric		Full Throughput Curves
Channel Geometry (CDL)	LCS UE	$\alpha = 180$, $\beta = 0$, $\gamma = 0$
	LCS gNB	$\alpha = 0$, $\beta = 10$, $\gamma = 0$
	GCS UE	Height = 1.5m; Azimuth = 0; X coordinate = 100m
	GCS gNB	Height = 25m; Azimuth = 0, X coordinate = 0
	gNB antenna polarisation	(-45, +45)
	gNB radiation pattern	Defined in Table 7.3-1 in TS 38.901
	UE antenna polarisation	(0, +90)
	UE radiation pattern	Omnidirectional
	Antenna panel placement	YZ Plane

Table B.2: Full standardised parameter table for PDSCH performance under SU-MIMO (FR1) from R4-2504616 [26]